Tensor-Based Spatial Smoothing (TB-SS) Using Multiple Snapshots

Arpita Thakre, *Student Member, IEEE*, Martin Haardt, *Senior Member, IEEE*, Florian Roemer, *Student Member, IEEE*, and K. Giridhar

***Abstract*—Tensor-based spatial smoothing (TB-SS) is a preprocessing technique for subspace-based parameter estimation of damped and undamped harmonics. In TB-SS, multichannel data is packed into a measurement tensor. We propose a tensor-based signal subspace estimation scheme that exploits the multidimensional invariance property exhibited by the highly structured measurement tensor. In the presence of noise, a tensor-based subspace estimate obtained via TB-SS is a better estimate of the desired signal subspace than the subspace estimate obtained by, for example, the singular value decomposition of a spatially smoothed matrix or a multilinear algebra approach reported in the literature. Thus, TB-SS in conjunction with subspace-based parameter estimation schemes performs significantly better than subspace-based parameter estimation algorithms applied to the existing matrix-based subspace estimate. Another advantage of TB-SS over the conventional SS is that TB-SS is insensitive to changes in the number of samples per subarray provided that the number of subarrays is greater than the number of harmonics. In this paper, we present, as an example, TB-SS in conjunction with ESPRIT-type algorithms for the parameter estimation of one-dimensional (1-D) damped and undamped harmonics. A closed form expression of the stochastic Cramér-Rao bound (CRB) for the 1-D damped harmonic retrieval problem is also derived.**

***Index Terms*—Damped harmonics, direction of arrival (DOA) estimation, higher-order tensor, higher-order singular value decomposition (HOSVD), multidimensional signal processing, multilinear algebra, parameter estimation, tensor-based spatial smoothing (TB-SS), tensor-ESPRIT.**

I. Introduction

DAMPED and undamped harmonic retrieval problems arise in several areas like mobile communications, sensor array processing, and nuclear magnetic resonance (NMR) spectroscopy [1]. The one-dimensional (1-D) undamped harmonic retrieval problem and the 1-D direction-of-arrival (DOA) estimation problem that use data from the output of a uniform linear array (ULA) of sensors have an identical data model. As a consequence, any preprocessing technique and subspace-based parameter estimation technique that can be applied to a 1-D undamped harmonic retrieval problem is also applicable to the 1-D DOA estimation problem. Spatial smoothing (SS) is a preprocessing technique used to increase the number of available snapshots and to decorrelate correlated wavefronts impinging on an array of sensors [2], [3]. In the context of damped and undamped harmonic retrieval problems, spatial smoothing is used to artificially increase the number of channels and to decorrelate correlated complex exponentials. ESPRIT [4] is a widely used subspace-based high-resolution technique for estimating the spatial frequencies of several sources impinging on the array of sensors. ESPRIT can also be used to estimate the normalized frequencies and the damping factors in a damped harmonic retrieval problem [5]. Unitary ESPRIT [6] exploits the centrosymmetry of a sensor array and enables computations in the real-valued domain, thereby reducing the complexity of ESPRIT. However, Unitary ESPRIT forces the phase factors of the complex exponentials to be on the unit circle and hence cannot be applied to a damped harmonic retrieval problem [5]. 1-D Unitary ESPRIT can be, therefore, used for estimating the normalized frequencies in an undamped harmonic retrieval problem and for estimating the spatial frequencies or DOAs in a 1-D DOA estimation problem. A disadvantage of conventional SS is that its performance in conjunction with subspace-based parameter estimation algorithms depends on the number of chosen subarrays.

In conventional spatial smoothing, the data corresponding to the artificially generated new channels (or snapshots) are stacked into the measurement matrix thereby forming a new matrix with an increased number of columns. Instead of doing this, packing spatially smoothed multichannel data into a multiway tensor reveals structure imposed by the spatial smoothing. The construction of a matrix-based subspace estimate from this highly structured measurement tensor using a higher-order singular value decomposition (HOSVD) based low rank approximation has been reported in [7]. However, this technique does not fully exploit the structure of the measurement tensor. In this paper, we propose a tensor-based subspace estimate that includes the core tensor and exploits the multidimensional invariance property exhibited by the measurement tensor. This tensor-based subspace estimate is thus an improved estimate of the signal subspace, thereby leading to an improved estimate of the normalized frequencies and the damping factors when tensor-based spatial smoothing (TB-SS) is used in conjunction with subspace-based parameter estimation techniques. In this paper, we use ESPRIT-type algorithms for estimating the normalized frequencies and the damping factors. However, this idea can be extended to other subspace-based parameter estimation schemes, such as, Matrix-Pencil, MUSIC, RARE [8].

Manuscript received March 31, 2009; accepted January 22, 2010. Date of publication February 17, 2010; date of current version April 14, 2010. The associate editor coordinating the review of this manuscript and approving it for publication was Dr. Xavier Mestre.

A. Thakre and K. Giridhar are with the Indian Institute of Technology Madras, India (e-mail: arpita@tenet.res.in; giri@tenet.res.in).

M. Haardt and F. Roemer are with the Ilmenau University of Technology, Germany (e-mail: martin.haardt@tu-ilmenau.de; florian.roemer@tu-ilmenau.de).

Color versions of one or more of the figures in this paper are available online at http://ieeexplore.ieee.org.

Digital Object Identifier 10.1109/TSP.2010.2043141

Important applications of the tensor-based methods include the estimation of the model parameters for the multidimensional harmonic model [9]. Multidimensional damped and undamped harmonic models have been studied in [10] and [11]. A tensor-based method for parameter estimation in the case of the damped and delayed sinusoidal model has been reported in [12]. Subspace based algorithms have been applied to nuclear magnetic resonance (NMR) data fitting problems also in [13]. We show that the structure of the data model we work with corresponds to a 2-D harmonic model with identical parameters along the two dimensions. In other words, we use a tensor-based method for solving a 1-D problem when more than one measurement snapshot is available. Note that a solution for the 1-D undamped harmonic retrieval problem with a single snapshot has been reported in [14].

We present the data model and the conventional SS in Sections II and III, respectively. We explain how and why to pack the noisy data in a tensor in Section IV. The existing matrix-based techniques are described in Section V. The proposed TB-SS for damped and undamped harmonic retrieval problems are explained in Sections VI and VII, respectively. Derivations for Cramér-Rao bounds (CRBs) are given in Section VIII. The simulation results are presented in Section IX. The paper concludes with Section X.

Notation

Scalars are denoted by italic letters $(a,\ b)$, column vectors by lower-case bold-face letters $(\boldsymbol{a},\ \boldsymbol{b})$, matrices by upper-case bold-face letters $(\boldsymbol{A},\ \boldsymbol{B})$ and tensors by calligraphic bold-face letters $(\boldsymbol{\mathcal{A}},\ \boldsymbol{\mathcal{B}})$. The ith element of the vector $\boldsymbol{a}$ is denoted by $[\boldsymbol{a}]_i$, the (i,j)th element of the matrix $\boldsymbol{A}$ by $[\boldsymbol{A}]_{i,j}$ and the jth column of the matrix $\boldsymbol{A}$ by $[\boldsymbol{A}]_{:,j}$. Let $(.)^H$, $(.)^T$, $(.)^*$, $E\{.\}$, $|.|$ correspond to the Hermitian transpose, the transpose, the conjugation, the expectation, and the modulus operator, respectively. The Kronecker product and the Khatri-Rao product (column-wise Kronecker product) of two matrices $\boldsymbol{A}$ and $\boldsymbol{B}$ are denoted as $\boldsymbol{A}\otimes\boldsymbol{B}$ and $\boldsymbol{A}\diamond\boldsymbol{B}$, respectively. The notation used for Hadamard-Schur (elementwise) product is $\odot$. The tensor operations we use are consistent with [15].

An n **mode vector** of an $(I_1\times I_2\times\cdots\times I_N)$-dimensional tensor $\boldsymbol{\mathcal{A}}$ is an I_n-dimensional vector obtained from $\boldsymbol{\mathcal{A}}$ by varying the index i_n and keeping the other indices fixed.

The **scalar product** of two tensors $\boldsymbol{\mathcal{A}},\ \boldsymbol{\mathcal{B}}\in\mathbb{C}^{I_1\times I_2\times\cdots\times I_N}$ is denoted by $\langle\boldsymbol{\mathcal{A}},\ \boldsymbol{\mathcal{B}}\rangle$ and computed by summing the element-wise product of $\boldsymbol{\mathcal{A}}$ and $\boldsymbol{\mathcal{B}}^*$ over all the indices, i.e.

$$c=\langle\boldsymbol{\mathcal{A}},\boldsymbol{\mathcal{B}}\rangle = \sum_{i_1=1}^{I_1}\sum_{i_2=1}^{I_2}\cdots\sum_{i_N=1}^{I_N} b^*_{i_1,i_2,\ldots,i_N}\cdot a_{i_1,i_2,\ldots,i_N}.$$

The n-**mode product** of a tensor $\boldsymbol{\mathcal{A}}\in\mathbb{C}^{I_1\times I_2\times\cdots\times I_N}$ and a matrix $\boldsymbol{U}\in\mathbb{C}^{J_n\times I_n}$ along the nth mode is denoted as

$$\boldsymbol{\mathcal{B}}=\boldsymbol{\mathcal{A}}\times_n\boldsymbol{U}\in\mathbb{C}^{I_1\times I_2\times\cdots\times I_{n-1}\times J_n\times I_{n+1}\times\cdots\times I_N}$$

$$b_{i_1,i_2,\ldots,i_{n-1},j_n,i_{n+1},\ldots i_N}=\sum_{i_n=1}^{I_n} a_{i_1,i_2,\ldots,i_N}\cdot u_{j_n,i_n}.$$

$[\boldsymbol{\mathcal{A}}]_{(n)}\in\mathbb{C}^{I_n\times I_1\cdot I_2\cdots I_{n-1}\cdot I_{n+1}\cdots I_N}$ is the matrix containing all the n-mode vectors of the tensor $\boldsymbol{\mathcal{A}}$ where the ordering of the columns is performed as in [15]. It is called the n-mode unfolding of the tensor $\boldsymbol{\mathcal{A}}$.

The **concatenation** of two tensors $\boldsymbol{\mathcal{A}}$ and $\boldsymbol{\mathcal{B}}$ along the nth mode is denoted by $[\boldsymbol{\mathcal{A}}\sqcup_n\boldsymbol{\mathcal{B}}]$.

The **higher-order SVD** (HOSVD) of a tensor $\boldsymbol{\mathcal{A}}\in\mathbb{C}^{I_1\times I_2\times\cdots\times I_N}$ is given by

$$\boldsymbol{\mathcal{A}}=\boldsymbol{\mathcal{C}}\times_1\boldsymbol{U}_1\times_2\boldsymbol{U}_2\cdots\times_N\boldsymbol{U}_N$$

where $\boldsymbol{\mathcal{C}}\in\mathbb{C}^{I_1\times I_2\times\cdots\times I_N}$ is the core tensor that satisfies the all-orthogonality conditions [15] and $\boldsymbol{U}_n\in\mathbb{C}^{I_n\times I_n}$, $n=1,2,\ldots,N$ are the unitary matrices of the n-mode singular vectors.

An identity tensor $\boldsymbol{\mathcal{I}}_{N,d}\in\mathbb{R}^{d\times d\times\cdots\times d}$ consists of elements $i_{i_1,i_2,\ldots,i_N}$ that satisfy

$$\begin{aligned} i_{i_1,i_2,\ldots,i_N}&=1 \text{ for } i_1=i_2=\cdots=i_N\\ &=0 \text{ otherwise.}\end{aligned}$$

Moreover, we denote $\boldsymbol{\Pi}_p$ as a $p\times p$ exchange matrix with ones on its antidiagonal and zeros elsewhere. We call $\boldsymbol{Q}\in\mathbb{C}^{p\times q}$ a left-$\boldsymbol{\Pi}$-real matrix if it satisfies $\boldsymbol{\Pi}_p\boldsymbol{Q}^*=\boldsymbol{Q}$. The unitary matrix

$$\boldsymbol{Q}_{2n+1}=\frac{1}{\sqrt{2}}\begin{bmatrix}\boldsymbol{I}_n & \boldsymbol{0} & j\boldsymbol{I}_n\\ \boldsymbol{0}^T & \sqrt{2} & \boldsymbol{0}^T\\ \boldsymbol{\Pi}_n & \boldsymbol{0} & -j\boldsymbol{\Pi}_n\end{bmatrix}$$

is left-$\boldsymbol{\Pi}$-real of odd order. A unitary left-$\boldsymbol{\Pi}$-real matrix of size $2n\times 2n$ is obtained from $\boldsymbol{Q}_{2n+1}$ by dropping its center row and center column.

A. Tensor Properties

Some of the tensor properties that we use in this paper are given below. For $n=1,2,\ldots,N$, see (1) at the bottom of the page, and

$$[\boldsymbol{\mathcal{I}}_{N,d}]_{(n)}\cdot(\boldsymbol{A}\otimes\boldsymbol{B}^T)=(\boldsymbol{A}^T\diamond\boldsymbol{B})^T \tag{2}$$

B. Terminology

The 1-D undamped harmonic retrieval problem and the 1-D DOA estimation problem that uses data from the output of a uniform linear array (ULA) of sensors have an identical data model. In Table I, we have listed a few variables that we use in this paper and their significance in the context of a harmonic

$$[\boldsymbol{\mathcal{A}}\times_1\boldsymbol{X}_1\times_2\boldsymbol{X}_2\cdots\times_N\boldsymbol{X}_N]_{(n)}=\boldsymbol{X}_n\cdot[\boldsymbol{\mathcal{A}}]_{(n)}\cdot(\boldsymbol{X}_{n+1}\otimes\boldsymbol{X}_{n+2}\cdots\boldsymbol{X}_N\otimes\boldsymbol{X}_1\cdots\otimes\boldsymbol{X}_{n-1})^T \tag{1}$$

TABLE I
MEANINGS OF VARIABLES

	Harmonic Retrieval	DOA Estimation
M	No. of samples	No. of sensors
N	No. of channels	No. of snapshots
d	No. of exponentials	No. of sources
$s_k(n)$	Complex amplitude of the kth cisoid in the nth channel	kth wavefront at the reference sensor at time n
μ_k	Normalized frequency	Spatial frequency

retrieval problem and a DOA estimation problem with a ULA [5].

II. Data Model

Assume a one-dimensional data sequence of d weighted and damped exponentials or harmonics in additive noise. The observation in the nth channel has the form

$$x_i(n) = \sum_{k=1}^{d} s_k(n) \mathrm{e}^{(\mathrm{j}\mu_k + \eta_k)i} + w_i(n) \tag{3}$$

for $i = 0, 1, 2, \ldots, (M-1),\ n = 1, 2, \ldots, N$. The normalized frequency is $\mu_k = 2\pi f_k T \in (-\pi, \pi]$, where f_k is the frequency of the kth exponential, η_k is the damping factor of the kth exponential, T is the sampling interval, and $s_k(n)$ is the complex amplitude of the kth exponential in the nth channel. The number of measurements or samples per channel is denoted by M, and N is the total number of channels. The M measurements from a channel are arranged in a vector and N such vectors form a matrix $\boldsymbol{X}$ as follows,

$$\boldsymbol{X} = \boldsymbol{A}\boldsymbol{S} + \boldsymbol{W} \quad \in \mathbb{C}^{M \times N}. \tag{4}$$

The entries of the noise matrix, $\boldsymbol{W}$, are assumed to be i.i.d., zero mean circularly symmetric complex Gaussian distributed with variance σ^2. The matrix $\boldsymbol{S} \in \mathbb{C}^{d \times N}$ denotes the complex signal matrix due to the d complex exponentials and the N channels. The Vandermonde matrix $\boldsymbol{A}$ is given by

$$\boldsymbol{A} = \left[\boldsymbol{o}\ (\boldsymbol{\Phi} \cdot \boldsymbol{o})\ (\boldsymbol{\Phi}^2 \cdot \boldsymbol{o})\ \ldots\ (\boldsymbol{\Phi}^{M-1} \cdot \boldsymbol{o})\right]^T$$

where

$$\begin{aligned} \boldsymbol{o}^T &= [1,\ 1,\ 1, \ldots, 1] \text{ and} \\ \boldsymbol{\Phi} &= \mathrm{diag}([e^{\mathrm{j}\mu_1 + \eta_1}, e^{\mathrm{j}\mu_2 + \eta_2}, \ldots, e^{\mathrm{j}\mu_d + \eta_d}]). \end{aligned} \tag{5}$$

Our aim is to estimate the normalized frequencies μ_k and the damping factors η_k for $k = 1, 2, \ldots, d$.

III. Spatial Smoothing

The array of M samples (or sensors) is divided into L subarrays, each having $M_{\mathrm{sub}} = M - L + 1$ samples (or sensors) to obtain a spatially smoothed matrix $\boldsymbol{X}_{\mathrm{ss}}$ from the measurement matrix $\boldsymbol{X}$ in (4) as depicted in Fig. 1. To this end we define the selection matrix of the lth subarray as

$$\boldsymbol{J}_\ell^{(M)} = [\boldsymbol{0}_{M_{\mathrm{sub}} \times (\ell-1)}\ \boldsymbol{I}_{M_{\mathrm{sub}}}\ \boldsymbol{0}_{M_{\mathrm{sub}} \times (L-\ell)}],\ 1 \le \ell \le L \tag{6}$$

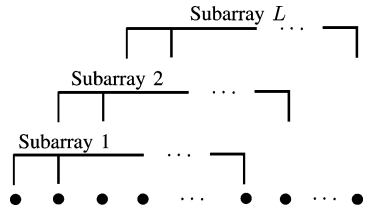

Fig. 1. Subarray choices for spatial smoothing. Subarray ℓ corresponds to the selection matrix $\boldsymbol{J}_\ell^{(M)}$, $1 \le \ell \le L$.

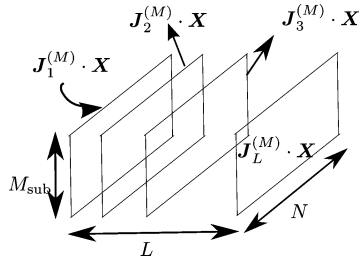

Fig. 2. Forming a three-way tensor $\boldsymbol{\mathcal{X}}$ from L submatrices.

such that

$$\begin{aligned} \boldsymbol{X}_{\mathrm{ss}} &= \left[\boldsymbol{J}_1^{(M)} \cdot \boldsymbol{X},\ \boldsymbol{J}_2^{(M)} \cdot \boldsymbol{X}, \ldots \boldsymbol{J}_L^{(M)} \cdot \boldsymbol{X}\right] \in \mathbb{C}^{M_{\mathrm{sub}} \times NL} \\ &= \left[\boldsymbol{J}_1^{(M)} \cdot \boldsymbol{A}\boldsymbol{S},\ \boldsymbol{J}_2^{(M)} \ldots \boldsymbol{A}\boldsymbol{S}, \ldots \boldsymbol{J}_L^{(M)} \cdot \boldsymbol{A}\boldsymbol{S}\right] \\ &\quad + \left[\boldsymbol{J}_1^{(M)} \cdot \boldsymbol{W},\ \boldsymbol{J}_2^{(M)} \cdot \boldsymbol{W}, \ldots \boldsymbol{J}_L^{(M)} \cdot \boldsymbol{W}\right] \\ &= \boldsymbol{A}_s \cdot \left[\boldsymbol{S},\ \boldsymbol{\Phi}\boldsymbol{S}, \ldots \boldsymbol{\Phi}^{L-1}\boldsymbol{S}\right] + \boldsymbol{W}_s \end{aligned} \tag{7}$$

where the Vandermonde matrix corresponding to the first subarray $\boldsymbol{A}_s$ is given by

$$\boldsymbol{A}_s = [\boldsymbol{I}_{M_{\mathrm{sub}}}\ \boldsymbol{0}_{M_{\mathrm{sub}} \times (M - M_{\mathrm{sub}})}]\boldsymbol{A} \quad \in \mathbb{C}^{M_{\mathrm{sub}} \times d} \tag{8}$$

We require that $M_{\mathrm{sub}} \ge d$ and $NL \ge d$ in order to estimate the d normalized frequencies and the d damping factors from $\boldsymbol{X}_{\mathrm{ss}}$. Each of the columns of the noise matrix $\boldsymbol{W}_s$ is white with $E\left\{[\boldsymbol{W}_s]_{:,k}[\boldsymbol{W}_s]_{:,k}^H\right\} = \sigma^2 \boldsymbol{I}_{M_{\mathrm{sub}}}$ and $E\left\{[\boldsymbol{W}_s]_{:,k}[\boldsymbol{W}_s]_{:,k}^T\right\} = \boldsymbol{0}_{M_{\mathrm{sub}} \times M_{\mathrm{sub}}}$ for $k = 1, 2, \ldots, NL$, but the columns of $\boldsymbol{W}_s$ are mutually correlated. Therefore, all the d spatial frequencies and the d damping factors can be estimated by applying ESPRIT-type algorithms to $\boldsymbol{X}_{\mathrm{ss}}$. Note that the effective number of samples per channel (or array aperture) reduces from M to M_{sub} and the number of effective channels (or snapshots) increases from N to NL due to spatial smoothing.

IV. Packing Measurement Samples Into a Tensor

In Section III, the spatially smoothed matrix $\boldsymbol{X}_{\mathrm{ss}}$ is formed by concatenating L submatrices where the ℓth submatrix is denoted by $\boldsymbol{J}_\ell^{(M)} \cdot \boldsymbol{X}$. Alternatively, these L submatrices can be placed along the second dimension of a tensor, as shown in Fig. 2, to form a three-way tensor $\boldsymbol{\mathcal{X}}$ given by

$$\boldsymbol{\mathcal{X}} = \boldsymbol{\mathcal{I}}_{3,d} \times_1 \boldsymbol{A}_s \times_2 \boldsymbol{B}_s \times_3 \boldsymbol{S}^T + \boldsymbol{\mathcal{W}} \quad \in \mathbb{C}^{M_{\mathrm{sub}} \times L \times N} \tag{9}$$

in which $\mathcal{I}_{3,d} \in \mathbb{C}^{d\times d\times d}$ is the identity tensor, $\boldsymbol{A}_s \in \mathbb{C}^{M_{\text{sub}}\times d}$ is defined in (8), $\boldsymbol{B}_s \in \mathbb{C}^{L\times d}$ contains the first L rows of the matrix $\boldsymbol{A}$, $\boldsymbol{S}^T \in \mathbb{C}^{N\times d}$, and $\boldsymbol{\mathcal{W}}$ is the noise component. In the absence of noise, the one-mode unfolding, the two-mode unfolding and the three-mode unfolding of the tensor $\boldsymbol{\mathcal{X}}$ are given by

$$[\boldsymbol{\mathcal{X}}]_{(1)} = \boldsymbol{A}_s \cdot (\boldsymbol{B}_s \diamond \boldsymbol{S}^T)^T \tag{10}$$

$$[\boldsymbol{\mathcal{X}}]_{(2)} = \boldsymbol{B}_s \cdot (\boldsymbol{S}^T \diamond \boldsymbol{A}_s)^T \tag{11}$$

$$[\boldsymbol{\mathcal{X}}]_{(3)} = \boldsymbol{S}^T \cdot (\boldsymbol{A}_s \diamond \boldsymbol{B}_s)^T. \tag{12}$$

It is evident that $[\boldsymbol{\mathcal{X}}]_{(1)}$ is same as (7) without the noise component $\boldsymbol{W}_s$.

The HOSVD [15] of the measurement tensor $\boldsymbol{\mathcal{X}}$ yields

$$\boldsymbol{\mathcal{X}} = \boldsymbol{\mathcal{C}} \times_1 \boldsymbol{U}_1 \times_2 \boldsymbol{U}_2 \times_3 \boldsymbol{U}_3 \tag{13}$$

where $\boldsymbol{\mathcal{C}} \in \mathbb{C}^{M_{\text{sub}}\times L\times N}$ is the core tensor, $\boldsymbol{U}_1 \in \mathbb{C}^{M_{\text{sub}}\times M_{\text{sub}}}$ are the left singular vectors of $[\boldsymbol{\mathcal{X}}]_{(1)}$, $\boldsymbol{U}_2 \in \mathbb{C}^{L\times L}$ are the left singular vectors of $[\boldsymbol{\mathcal{X}}]_{(2)}$, and $\boldsymbol{U}_3 \in \mathbb{C}^{N\times N}$ are the left singular vectors of $[\boldsymbol{\mathcal{X}}]_{(3)}$.

In the absence of noise, $\boldsymbol{\mathcal{X}}$ can be expressed in terms of an "economy size" HOSVD in the following way:

$$\boldsymbol{\mathcal{X}} = \boldsymbol{\mathcal{C}}^{[s]} \times_1 \boldsymbol{U}_1^{[s]} \times_2 \boldsymbol{U}_2^{[s]} \times_3 \boldsymbol{U}_3^{[s]} \tag{14}$$

where $\boldsymbol{\mathcal{C}}^{[s]} \in \mathbb{C}^{\min(d,M_{\text{sub}})\times\min(d,L)\times\min(d,N)}$, $\boldsymbol{U}_1^{[s]} \in \mathbb{C}^{M_{\text{sub}}\times\min(d,M_{\text{sub}})}$ are the $\min(d, M_{\text{sub}})$ dominant left singular vectors of $[\boldsymbol{\mathcal{X}}]_{(1)}$, $\boldsymbol{U}_2^{[s]} \in \mathbb{C}^{L\times\min(d,L)}$ are the $\min(d, L)$ dominant left singular vectors of $[\boldsymbol{\mathcal{X}}]_{(2)}$, and $\boldsymbol{U}_3^{[s]} \in \mathbb{C}^{N\times\min(d,N)}$ are the $\min(d, N)$ dominant left singular vectors of $[\boldsymbol{\mathcal{X}}]_{(3)}$. Given that $(j\mu_k + \eta_k)$ are distinct for $k = 1, 2, \ldots, d$, the columns of $\boldsymbol{U}_1^{[s]}$ span the column space spanned by $\boldsymbol{A}_s$ provided $M_{\text{sub}} \geq d$ and the columns of $\boldsymbol{U}_2^{[s]}$ span the column space spanned by $\boldsymbol{B}_s$ provided $L \geq d$. Under the assumption $M_{\text{sub}} \geq d$ and $L \geq d$, there exist two nonsingular $d \times d$ complex matrices $\boldsymbol{T}_1$ and $\boldsymbol{T}_2$ such that

$$\boldsymbol{A}_s = \boldsymbol{U}_1^{[s]}\boldsymbol{T}_1, \quad \boldsymbol{B}_s = \boldsymbol{U}_2^{[s]}\boldsymbol{T}_2. \tag{15}$$

In the presence of noise, $\boldsymbol{\mathcal{C}}^{[s]}$, $\boldsymbol{U}_1^{[s]}$, $\boldsymbol{U}_2^{[s]}$, $\boldsymbol{U}_3^{[s]}$ can be estimated by any HOSVD-based low-rank approximation of $\boldsymbol{\mathcal{X}}$, e.g., the Higher Order Orthogonal Iteration (HOOI) algorithm described in [16] or the truncated HOSVD described in [15].

V. Existing Approaches for Parameter Estimation

In this section, we briefly review the algorithms that are used as a comparison to the presented TB-SS technique.

A. 1-D Standard ESPRIT

We can solve for $\boldsymbol{\Phi}$ from the spatially smoothed matrix $\boldsymbol{X}_{\text{ss}}$ using 1-D standard ESPRIT [4].

B. Method Proposed in [7]

Observe that both $\boldsymbol{A}_s$ and $\boldsymbol{B}_s$ satisfy the shift invariance property and we can write

$$\boldsymbol{J}_1^{(1)}\boldsymbol{A}_s\boldsymbol{\Phi} = \boldsymbol{J}_2^{(1)}\boldsymbol{A}_s$$

$$\boldsymbol{J}_1^{(2)}\boldsymbol{B}_s\boldsymbol{\Phi} = \boldsymbol{J}_2^{(2)}\boldsymbol{B}_s. \tag{16}$$

If two subarrays of maximum overlap are selected, then

$$\begin{aligned}\boldsymbol{J}_1^{(1)} &= [\boldsymbol{I}_{M_{\text{sub}}-1}\ \boldsymbol{0}_{(M_{\text{sub}}-1)\times 1}]\\ \boldsymbol{J}_2^{(1)} &= [\boldsymbol{0}_{(M_{\text{sub}}-1)\times 1}\ \boldsymbol{I}_{M_{\text{sub}}-1}]\\ \boldsymbol{J}_1^{(2)} &= [\boldsymbol{I}_{L-1}\ \boldsymbol{0}_{(L-1)\times 1}]\\ \boldsymbol{J}_2^{(2)} &= [\boldsymbol{0}_{(L-1)\times 1}\ \boldsymbol{I}_{L-1}]\end{aligned} \tag{17}$$

$\boldsymbol{A}_s$ and $\boldsymbol{B}_s$ in (16) can be replaced by $\boldsymbol{U}_1^{[s]}$ and $\boldsymbol{U}_2^{[s]}$, respectively, as shown

$$\boldsymbol{J}_1^{(1)}\boldsymbol{U}_1^{[s]}\boldsymbol{\Psi}_1 = \boldsymbol{J}_2^{(1)}\boldsymbol{U}_1^{[s]} \tag{18}$$

$$\boldsymbol{J}_1^{(2)}\boldsymbol{U}_2^{[s]}\boldsymbol{\Psi}_2 = \boldsymbol{J}_2^{(2)}\boldsymbol{U}_2^{[s]} \tag{19}$$

where $\boldsymbol{\Psi}_1 = \boldsymbol{T}_1\boldsymbol{\Phi}\boldsymbol{T}_1^{-1}$ and $\boldsymbol{\Psi}_2 = \boldsymbol{T}_2\boldsymbol{\Phi}\boldsymbol{T}_2^{-1}$. The above two overdetermined equations hold only approximately in the presence of noise. These equations can be solved for $\boldsymbol{\Psi_1}$ and $\boldsymbol{\Psi_2}$, respectively, using least squares (LS), total least squares (TLS), or structured least squares (SLS) [17]. The TLS solution of (18) is given by

$$\boldsymbol{\Psi}_1 = -\boldsymbol{W}_{12}\boldsymbol{W}_{22}^{-1} \tag{20}$$

where $\boldsymbol{W} = \begin{bmatrix}\boldsymbol{W}_{11} & \boldsymbol{W}_{12}\\ \boldsymbol{W}_{21} & \boldsymbol{W}_{22}\end{bmatrix}$ contains the right singular vectors of the matrix $[\boldsymbol{J}_1^{(1)}\boldsymbol{U}_1^{[s]},\ \boldsymbol{J}_2^{(1)}\boldsymbol{U}_1^{[s]}] \in \mathbb{C}^{(M_{\text{sub}}-1)\times 2d}$. The normalized frequencies and the damping factors are determined from $\boldsymbol{\Psi}_1$ in the following way:

$$\eta_k = \ln(|\lambda_k|) \tag{21a}$$

$$\mu_k = \arg(\lambda_k) \quad \text{for} \quad k = 1, 2, \ldots, d \tag{21b}$$

where λ_k is the kth eigenvalue of the matrix $\boldsymbol{\Psi}_1$. The authors of [7] apply the HOOI algorithm to find an estimate of $\boldsymbol{U}_1^{[s]}$ from the tensor $\boldsymbol{\mathcal{X}}$ and determine the normalized frequencies $\mu_1,\ \mu_2, \ldots \mu_d$ by solving (18) using TLS.

C. 2-D Standard ESPRIT

We can apply 2-D standard ESPRIT to the matrix $[\boldsymbol{\mathcal{X}}]_{(3)}^T$. The difference to a standard 2-D harmonic retrieval problem is that here the parameters along the two dimensions are the same. We therefore start by applying a SVD to the matrix $[\boldsymbol{\mathcal{X}}]_{(3)}$ and solve for the unknown parameters as explained below. The SVD of the matrix $[\boldsymbol{\mathcal{X}}]_{(3)}$ is given by

$$[\boldsymbol{\mathcal{X}}]_{(3)} = \boldsymbol{U}_3\boldsymbol{\Sigma}_3\boldsymbol{V}_3^H. \tag{22}$$

An "economy-size" SVD of the matrix $[\boldsymbol{\mathcal{X}}]_{(3)}^T$ will be

$$[\boldsymbol{\mathcal{X}}]_{(3)}^T = \boldsymbol{V}_3^{*[s]}\boldsymbol{\Sigma}_3^{[s]}\boldsymbol{U}_3^{T[s]} \tag{23}$$

where $\boldsymbol{V}_3^{*[s]} \in \mathbb{C}^{M_{\text{sub}}L\times\min(d,M_{\text{sub}}L)}$ spans the subspace spanned by $\boldsymbol{C}_s = (\boldsymbol{A}_s \diamond \boldsymbol{B}_s)$. For some nonsingular matrix $\boldsymbol{T}_3 \in \mathbb{C}^{d\times d}$, $\boldsymbol{C}_s = \boldsymbol{V}_3^{*[s]}\boldsymbol{T}_3$. The complex-valued matrices $\boldsymbol{\Sigma}_3^{[s]}$ and $\boldsymbol{U}_3^{T[s]}$ are of size $\min(d, M_{\text{sub}}L) \times \min(d, N)$ and

$\min(d, N) \times N$, respectively. The matrix $\boldsymbol{\Phi}$ satisfies the following equations:

$$(\boldsymbol{J}_1^{(1)} \otimes \boldsymbol{I}_L)\boldsymbol{C}_s\boldsymbol{\Phi} = (\boldsymbol{J}_2^{(1)} \otimes \boldsymbol{I}_L)\boldsymbol{C}_s$$
$$(\boldsymbol{I}_{M_{\text{sub}}} \otimes \boldsymbol{J}_1^{(2)})\boldsymbol{C}_s\boldsymbol{\Phi} = (\boldsymbol{I}_{M_{\text{sub}}} \otimes \boldsymbol{J}_2^{(2)})\boldsymbol{C}_s. \quad (24)$$

As in the standard ESPRIT algorithm, we solve for $\boldsymbol{\Psi}_b$ using one of the following equations:

$$(\boldsymbol{J}_1^{(1)} \otimes \boldsymbol{I}_L)\boldsymbol{V}_3^{*[s]}\boldsymbol{\Psi}_b = (\boldsymbol{J}_2^{(1)} \otimes \boldsymbol{I}_L)\boldsymbol{V}_3^{*[s]} \quad (25)$$
$$(\boldsymbol{I}_{M_{\text{sub}}} \otimes \boldsymbol{J}_1^{(2)})\boldsymbol{V}_3^{*[s]}\boldsymbol{\Psi}_b = (\boldsymbol{I}_{M_{\text{sub}}} \otimes \boldsymbol{J}_2^{(2)})\boldsymbol{V}_3^{*[s]} \quad (26)$$

where $\boldsymbol{\Psi}_b = \boldsymbol{T}_3\boldsymbol{\Phi}\boldsymbol{T}_3^{-1}$. We propose to solve (25) if $M_{\text{sub}} \geq L$ or solve (26) if $M_{\text{sub}} < L$.

VI. Proposed Tensor-Based Approach for Damped Harmonic Retrieval Problem

The measurement tensor $\boldsymbol{\mathcal{X}}$ from (10) can be written as

$$\boldsymbol{\mathcal{X}} = \boldsymbol{\mathcal{A}} \times_3 \boldsymbol{S}^T + \boldsymbol{\mathcal{W}} \quad (27)$$

where $\boldsymbol{\mathcal{A}} \in \mathbb{C}^{M_{\text{sub}} \times L \times d}$ is a tensor that exhibits shift-invariances in its first mode and in its second mode in the absence of noise. Writing the invariance (16) in tensor notation yields

$$\boldsymbol{\mathcal{A}} \times_1 \boldsymbol{J}_1^{(1)} \times_3 \boldsymbol{\Phi} = \boldsymbol{\mathcal{A}} \times_1 \boldsymbol{J}_2^{(1)}$$
$$\boldsymbol{\mathcal{A}} \times_2 \boldsymbol{J}_1^{(2)} \times_3 \boldsymbol{\Phi} = \boldsymbol{\mathcal{A}} \times_2 \boldsymbol{J}_2^{(2)} \quad (28)$$

where $\boldsymbol{J}_i^{(r)}$ is the ith real selection matrix for the rth mode and is given by (17). Here, $r = 1$ corresponds to the first mode and $r = 2$ corresponds to the second mode.

We exploit the shift invariance of $\boldsymbol{\mathcal{A}}$ in two of its three modes. To this end we define a tensor $\boldsymbol{\mathcal{U}}^{[s]}$ in the following way [9]:

$$\boldsymbol{\mathcal{U}}^{[s]} = \boldsymbol{\mathcal{C}}^{[s]} \times_1 \boldsymbol{U}_1^{[s]} \times_2 \boldsymbol{U}_2^{[s]} \quad \in \mathbb{C}^{M_{\text{sub}} \times L \times d}. \quad (29)$$

In the absence of noise and for $N \geq d$ or with an infinite number of channels, N, (snapshots in the context of DOA estimation problem) the vector space spanned by the one-mode vectors and the two-mode vectors of $\boldsymbol{\mathcal{A}}$ and $\boldsymbol{\mathcal{U}}^{[s]}$ are equal. Therefore there exists a nonsingular complex matrix $\boldsymbol{T} \in \mathbb{C}^{d \times d}$, for $N \geq d$, such that

$$\boldsymbol{\mathcal{A}} = \boldsymbol{\mathcal{U}}^{[s]} \times_3 \boldsymbol{T}. \quad (30)$$

The unknown tensor $\boldsymbol{\mathcal{A}}$ is eliminated from (28) by applying (30) to get

$$\boldsymbol{\mathcal{U}}^{[s]} \times_1 \boldsymbol{J}_1^{(1)} \times_3 \boldsymbol{\Psi} = \boldsymbol{\mathcal{U}}^{[s]} \times_1 \boldsymbol{J}_2^{(1)} \quad (31)$$
$$\boldsymbol{\mathcal{U}}^{[s]} \times_2 \boldsymbol{J}_1^{(2)} \times_3 \boldsymbol{\Psi} = \boldsymbol{\mathcal{U}}^{[s]} \times_2 \boldsymbol{J}_2^{(2)} \quad (32)$$

where $\boldsymbol{\Psi} = \boldsymbol{T}^{-1}\boldsymbol{\Phi}\boldsymbol{T}$. With a finite number of channels and in the presence of noise, (31) and (32) hold only approximately. These equations can be solved using LS [9], TLS or tensor-structure structured least-squares (TS-SLS) [18]. There is no restriction on M_{sub} and L except that they cannot both be less than $(d+1)$. In the presence of noise, $\boldsymbol{\mathcal{C}}^{[s]}$, $\boldsymbol{U}_1^{[s]}$, and $\boldsymbol{U}_2^{[s]}$ are obtained from the noise corrupted measurement tensor $\boldsymbol{\mathcal{X}}$ via any HOSVD-based rank-$(\min(d, M_{\text{sub}}), \min(d, L), d)$ approximation of $\boldsymbol{\mathcal{X}}$.

Taking the third unfolding of the tensors on both sides of the (31), we get

$$(\boldsymbol{J}_1^{(1)} \otimes \boldsymbol{I}_L) \cdot [\boldsymbol{\mathcal{U}}^{[s]}]_{(3)}^T \cdot \boldsymbol{\Psi}^T = (\boldsymbol{J}_2^{(1)} \otimes \boldsymbol{I}_L) \cdot [\boldsymbol{\mathcal{U}}^{[s]}]_{(3)}^T. \quad (33)$$

It is evident after comparing (25) with the above equation that the matrix $[\boldsymbol{\mathcal{U}}^{[s]}]_{(3)}^T$ replaces the matrix $\boldsymbol{V}_3^{*[s]}$, where $[\boldsymbol{\mathcal{U}}^{[s]}]_{(3)}^T$ is given by

$$[\boldsymbol{\mathcal{U}}^{[s]}]_{(3)}^T = (\boldsymbol{U}_1^{[s]} \otimes \boldsymbol{U}_2^{[s]})[\boldsymbol{\mathcal{C}}^{[s]}]_{(3)}^T$$
$$= (\boldsymbol{U}_1^{[s]} \otimes \boldsymbol{U}_2^{[s]}) \cdot \boldsymbol{U}_D \cdot \boldsymbol{\Sigma}_3^{[s]} \quad (34)$$

and the matrix $\boldsymbol{U}_D \in \mathbb{C}^{d^2 \times d}$ has orthonormal columns. The matrix $\boldsymbol{U}_D$ is a normalized version of the third unfolding of the truncated core tensor $\boldsymbol{\mathcal{C}}^{[s]}$. The matrix $\boldsymbol{\Sigma}_3^{[s]}$ is a diagonal matrix, where the diagonal entries are the first d singular values of the matrix $[\boldsymbol{\mathcal{X}}]_{(3)}^T$. Note that the diagonal entries of $\boldsymbol{\Sigma}_3^{[s]}$ are the two-norms of the column vectors of $\boldsymbol{V}_3^{*[s]}$.

In the HOSVD-based low-rank approximation, the truncation is done in all three modes separately while in the SVD-based low rank approximation truncation is only performed in the last mode. This removes more noise power and, hence, enhances the subspace. In the same way, in the HOOI-based low-rank approximation, low-rank approximations of all the three unfoldings of the three-way tensor are computed iteratively thereby leading to noise power reduction.

The authors in [19] have derived a relation between the HOSVD-based subspace estimate and the SVD-based subspace estimate. They have shown that in the presence of noise

$$\left[\boldsymbol{\mathcal{U}}^{[s]}\right]_{(3)}^T = (\boldsymbol{Z}_1 \otimes \boldsymbol{Z}_2)\,\boldsymbol{V}_3^{*[s]}. \quad (35)$$

The matrix-based subspace estimate $\boldsymbol{V}_3^{*[s]}$ gets premultiplied by a Kronecker product of $\boldsymbol{Z}_1$ and $\boldsymbol{Z}_2$, which are the projection matrices onto the subspaces spanned be the one-mode and the two-mode vectors of $\boldsymbol{\mathcal{U}}^{[s]}$. Therefore, the matrix-based subspace estimate is "projected into the Kronecker structure," which does reduce the error since it enforces more of the structure the true subspace features.

The above facts lead to a significant improvement in the estimation of the normalized frequencies, μ_k and the damping factors, η_k for $k = 1, 2, \ldots, d$, using $\boldsymbol{\mathcal{U}}^{[s]}$ as it is evident from the simulation results. We measure the closeness of the estimated signal subspace to the true signal subspace in terms of largest principal angle (LPA).

There are two reasons why TB-SS in conjunction with ESPRIT type algorithms provides a lower root mean square error in the estimated parameters than 1-D ESPRIT and the method proposed in [7]. The first reason is that the tensor-based estimated signal subspace is better than the SVD-based subspace estimate obtained in 1-D ESPRIT. The second reason is that in TB-SS we solve $(M_{\text{sub}} - 1)L$ or $(L - 1)M_{\text{sub}}$ equations, depending on the values of M_{sub} and L, to estimate d parameters, while in 1-D ESPRIT and in the method proposed in [7] we solve $(M_{\text{sub}} - 1)$ equations to estimate d parameters.

Both the (18) and (19) contain information about $\boldsymbol{\Phi}$. In equivalent tensor notation, both (31) and (32) contain information about $\boldsymbol{\Phi}$. We can therefore, estimate $\boldsymbol{\Phi}$ either by solving (31)

or (32) or both. However combining (31) and (32) leads to averaging thereby giving a performance in between the performances given by (31) and (32). Equation(31) has $(M_{\rm sub}-1)L$ equations and d unknowns while (32) has $(L-1)M_{\rm sub}$ equations and d unknowns. We therefore solve (31) if $M_{\rm sub} \geq L$ or (32) if $M_{\rm sub} < L$. We propose an *a priori* rule to decide which of the two (31) and (32) should be used to estimate the parameters and why. Simulations are not needed to figure out whether to use (31) or (32) in a specific scenario. The above method of estimating the normalized frequencies and the damping factors using the shift-invariance property of the highly structured tensor $\boldsymbol{\mathcal{A}}$ is called standard Tensor-ESPRIT [9].

The LS solution of (31) [or (32)] is given by [9]

$$\begin{aligned}\boldsymbol{\Psi}^T &= \left(\boldsymbol{\Xi}_1^{(r)} \cdot [\boldsymbol{\mathcal{U}}^{[s]}]_{(3)}^T\right)^+ \cdot \boldsymbol{\Xi}_2^{(r)} \cdot [\boldsymbol{\mathcal{U}}^{[s]}]_{(3)}^T \quad \in \mathbb{C}^{d\times d}\\ \boldsymbol{\Xi}_1^{(1)} &= \boldsymbol{J}_1^{(1)} \otimes \boldsymbol{I}_L,\ \boldsymbol{\Xi}_2^{(1)} = \boldsymbol{J}_2^{(1)} \otimes \boldsymbol{I}_L, \quad \text{for } r=1,\\ \boldsymbol{\Xi}_1^{(2)} &= \boldsymbol{I}_{M_{\rm sub}} \otimes \boldsymbol{J}_1^{(2)},\ \boldsymbol{\Xi}_2^{(2)} = \boldsymbol{I}_{M_{\rm sub}} \otimes \boldsymbol{J}_2^{(2)}, \quad \text{for } r=2.\end{aligned} \tag{36}$$

Here, $r=1$ corresponds to (31) and $r=2$ corresponds to (32).

The TS-SLS algorithm for (31) [or (32)] starts with the LS solution of (31) [or (32)] and then the solution is improved by an iterative procedure [18]. The number of iterations required is typically one to three.

We use the tensor-based subspace estimate $\boldsymbol{\mathcal{U}}^{[s]}$ that contains the core tensor $\boldsymbol{\mathcal{C}}^{[s]}$ to estimate the unknown parameters, i.e., the normalized frequencies and the damping factors. Therefore the spatial smoothing and the subspace estimation technique proposed in this paper is a tensor-based approach.

VII. Proposed Tensor-Based Approach for Undamped Harmonic Retrieval Problem

Forward-backward (F-B) averaging can be applied to the spatially smoothed measurement matrix $\boldsymbol{X}_{\rm ss}$ and the measurement tensor $\boldsymbol{\mathcal{X}}$ for the undamped harmonic retrieval case, i.e., when $\eta_k = 0$ for $k = 1,2,\ldots,d$. In the context of DOA estimation problem, F-B averaging can be applied to $\boldsymbol{X}_{\rm ss}$ provided the sensor array is centro-symmetric.

The forward-backward averaged and the spatially smoothed measurement matrix $\boldsymbol{X}_{\rm ss}^{\rm (fba)}$ is given by

$$\boldsymbol{X}_{\rm ss}^{\rm (fba)} = [\boldsymbol{X}_{\rm ss}\ \ \boldsymbol{\Pi}_{M_{\rm sub}} \boldsymbol{X}_{\rm ss}^* \boldsymbol{\Pi}_{NL}] \quad \in \mathbb{C}^{M_{\rm sub}\times 2NL}. \tag{37}$$

The forward-backward averaged measurement tensor $\boldsymbol{\mathcal{X}}^{\rm (fba)}$ is given by [9]

$$\boldsymbol{\mathcal{X}}^{\rm (fba)} = [\boldsymbol{\mathcal{X}}_{\sqcup 3}(\boldsymbol{\mathcal{X}}^* \times_1 \boldsymbol{\Pi}_{M_{\rm sub}} \times_2 \boldsymbol{\Pi}_L \times_3 \boldsymbol{\Pi}_N)] \quad \in \mathbb{C}^{M_{\rm sub}\times L\times 2N}. \tag{38}$$

The effective number of data samples doubles due to forward-backward averaging. For the undamped harmonic retrieval problem, we proceed with the matrix $\boldsymbol{X}_{\rm ss}^{\rm (fba)}$ or the tensor $\boldsymbol{\mathcal{X}}^{\rm (fba)}$ as described in Section VI to estimate the d normalized frequencies (d spatial frequencies in case of DOA estimation problem). Alternatively, Unitary ESPRIT can be applied to $\boldsymbol{X}_{\rm ss}$ and Unitary Tensor-ESPRIT [9] can be applied to $\boldsymbol{\mathcal{X}}$. The Unitary Tensor-ESPRIT (Unitary ESPRIT) algorithm incorporates forward-backward averaging. Therefore the performance of Unitary Tensor-ESPRIT applied to $\boldsymbol{\mathcal{X}}$ (Unitary ESPRIT applied to $\boldsymbol{X}_{\rm ss}$) is similar to the performance of standard Tensor-ESPRIT applied to $\boldsymbol{\mathcal{X}}^{\rm (fba)}$ (standard ESPRIT applied to $\boldsymbol{X}_{\rm ss}^{\rm (fba)}$). The advantage of Unitary Tensor-ESPRIT (Unitary ESPRIT) over standard Tensor-ESPRIT (standard ESPRIT) is that it performs all the computations in the real-valued domain thereby reducing the computational complexity of the algorithm significantly. We need to make sure that $N/2 \geq d$ for the undamped harmonic retrieval problem.

TABLE II
Restrictions on the Parameters

	Damped & Undamped Harmonic Retrieval	Damped Retrieval Retrieval	Undamped Harmonic Retrieval
1-D ESPRIT	$M_{\rm sub} \geq (d+1)$	$NL \geq d$	$NL \geq \frac{d}{2}$
Method of [7]	$M_{\rm sub} \geq (d+1)$	$N \geq d$	$N \geq \frac{d}{2}$
2-D ESPRIT	$M_{\rm sub}L \geq (d+1)$	$N \geq d$	$N \geq \frac{d}{2}$
TB-SS	$M_{\rm sub} \geq (d+1)$ or $L \geq (d+1)$	$N \geq d$	$N \geq \frac{d}{2}$

A rank-$(\min(d, M_{\rm sub}),\ \min(d, L)),\ d)$ approximation of $\varphi(\boldsymbol{\mathcal{X}})$, as defined in [9], and denoted as $\boldsymbol{\mathcal{Z}}$, is determined using any HOSVD-based low-rank approximation technique. The tensor $\boldsymbol{\mathcal{Z}}$ is given by

$$\boldsymbol{\mathcal{Z}} = \boldsymbol{\mathcal{C}}_Z^{[s]} \times_1 \boldsymbol{E}_1^{[s]} \times_2 \boldsymbol{E}_2^{[s]} \times_3 \boldsymbol{E}_3^{[s]} \quad \in \mathbb{R}^{M_{\rm sub}\times L\times 2N}. \tag{39}$$

Similar to (29), a real-valued tensor-based subspace estimate $\boldsymbol{\mathcal{E}}^{[s]}$ is formed as follows:

$$\boldsymbol{\mathcal{E}}^{[s]} = \boldsymbol{\mathcal{C}}_Z^{[s]} \times_1 \boldsymbol{E}_1^{[s]} \times_2 \boldsymbol{E}_2^{[s]} \quad \in \mathbb{R}^{M_{\rm sub}\times L\times d}. \tag{40}$$

In the absence of noise, the real-valued shift invariance equations satisfied by the one-mode vectors and the two-mode vectors of $\boldsymbol{\mathcal{E}}^{[s]}$ are

$$\boldsymbol{\mathcal{E}}^{[s]} \times_1 \boldsymbol{K}_1^{(1)} \times_3 \boldsymbol{\Upsilon} = \boldsymbol{\mathcal{E}}^{[s]} \times_1 \boldsymbol{K}_2^{(1)} \tag{41}$$

$$\boldsymbol{\mathcal{E}}^{[s]} \times_2 \boldsymbol{K}_1^{(2)} \times_3 \boldsymbol{\Upsilon} = \boldsymbol{\mathcal{E}}^{[s]} \times_2 \boldsymbol{K}_2^{(2)}. \tag{42}$$

The matrices $\boldsymbol{\Omega} = \operatorname{diag}\{\tan(\mu_k/2)\}_{k=1}^d$ and $\boldsymbol{\Upsilon}$ are related through a similarity transformation. We suggest in this paper to solve (41) if $M_{\rm sub} \geq L$ or (42) if $M_{\rm sub} < L$ for estimating the normalized (or spatial) frequencies $\mu_1,\ \mu_2, \ldots \mu_d$. The detail of the algorithm is omitted here due to lack of space. The LS solutions of (41) and (42) are given in [9]. The TS-SLS solution is explained in [18].

Table II shows the restrictions on the values of the parameters $M_{\rm sub}$, L and N for the existing approaches and the tensor-based approach TB-SS presented in this paper. Table III displays the computational complexity of the algorithms.

VIII. CRB

For the damped harmonic retrieval case, we define $\boldsymbol{D} = [\partial \boldsymbol{a}_1/\partial\mu_1, \partial \boldsymbol{a}_2/\partial\mu_2, \ldots, \partial \boldsymbol{a}_d/\partial\mu_d, \partial \boldsymbol{a}_1/\partial\eta_1, \ldots, \partial \boldsymbol{a}_d/\partial\eta_d]$ where $\boldsymbol{a}_i$ is the ith column of $\boldsymbol{A}$. We also define $\boldsymbol{R}_{\rm ss} = [\boldsymbol{R}_s,\ \boldsymbol{R}_s]$. It is shown in the Appendix that the stochastic CRB is given by

$$\text{CRB}(\boldsymbol{\beta}) = \frac{\sigma^2}{2N} \cdot \operatorname{Re}\left\{(\boldsymbol{D}^H \boldsymbol{P}_{\boldsymbol{A}} \boldsymbol{D}) \odot (\boldsymbol{R}_{\rm ss} \boldsymbol{A}^H \boldsymbol{R}_x^{-1} \boldsymbol{A} \boldsymbol{R}_{\rm ss})^T\right\}^{-1}. \tag{43}$$

TABLE III
COMPUTATIONAL COMPLEXITY

	No. of SVDs	Size of overdetermined set of equations
1-D ESPRIT	1	$(M_{\rm sub}-1)\times d$
Method of [7]	3	$(M_{\rm sub}-1)\times d$
2-D ESPRIT	1	$(M_{\rm sub}-1)L\times d$
TB-SS	3	$(M_{\rm sub}-1)L\times d$ or $M_{\rm sub}(L-1)\times d$

For the definitions of the other parameters, refer to the Appendix. For the undamped harmonic retrieval case a closed form expression for the stochastic CRB can be found in [20].

IX. SIMULATION RESULTS

We use standard Tensor-ESPRIT (or standard ESPRIT) to estimate the normalized frequencies and the damping factors in the damped harmonic retrieval problem and use Unitary Tensor-ESPRIT (or Unitary ESPRIT) for estimating the normalized (or spatial) frequencies in the undamped harmonic retrieval problem. For damped harmonic retrieval problem, the estimates of the tensor $\boldsymbol{\mathcal{C}}^{[s]}$ and the matrices $\boldsymbol{U}_1^{[s]},\boldsymbol{U}_2^{[s]}$ can be obtained from the measurement tensor $\boldsymbol{\mathcal{X}}$ using: a) the HOOI algorithm or b) the truncated HOSVD. For undamped harmonic retrieval problem, the estimates of $\boldsymbol{\mathcal{C}}_Z^{[s]},\boldsymbol{E}_1^{[s]},\boldsymbol{E}_2^{[s]}$ can be obtained from $\varphi(\boldsymbol{\mathcal{X}})$ via a) the HOOI algorithm or b) the truncated HOSVD. In this paper, six approaches have been compared in terms of the root mean square error (RMSE). The RMSEs are defined as

$$\text{RMSE}(\mu)=\sqrt{\frac{1}{R}\sum_{i=1}^{R}\sum_{k=1}^{d}\left(\mu_k^{(i)}-\hat{\mu}_k^{(i)}\right)^2}$$

$$\text{RMSE}(\eta)=\sqrt{\frac{1}{R}\sum_{i=1}^{R}\sum_{k=1}^{d}\left(\eta_k^{(i)}-\hat{\eta}_k^{(i)}\right)^2}$$

where $\hat{\mu}_k$, $\hat{\eta}_k$ are the kth estimated normalized frequency and the kth estimated damping factor, respectively, and R is the number of runs. The first approach is without spatial smoothing (SS), i.e., estimating the unknown parameters from the matrix $\boldsymbol{X}$ using standard ESPRIT with TLS. In the second approach the parameters are estimated from the spatially smoothed matrix $\boldsymbol{X}_{\rm ss}$ using 1-D standard ESPRIT with TLS. The third approach is the approach from [7] where the measurement samples are packed into the measurement tensor $\boldsymbol{\mathcal{X}}$ and the parameters are estimated from the unitary matrix of the one-mode singular vectors, i.e., $\boldsymbol{U}_1^{[s]}$, using standard ESPRIT with TLS. The fourth one is estimating the parameters by applying 2-D standard ESPRIT to the matrix $[\boldsymbol{\mathcal{X}}]_3^T$. The fifth and the sixth approaches are the TB-SS approaches. The fifth one is TB-SS with standard Tensor-ESPRIT and LS approach in which the enhanced tensor-based subspace estimate $\boldsymbol{\mathcal{U}}^{[s]}$ is formed from the measurement tensor $\boldsymbol{\mathcal{X}}$ and standard Tensor-ESPRIT is used to solve the invariance (31) or (32) via LS. The sixth and the last one is TB-SS with standard Tensor-ESPRIT and TS-SLS which is same as the fifth approach except that the TS-SLS algorithm is used instead of LS to solve the invariance (31) or (32). While applying the TS-SLS, we set the maximum number of iterations to 3. Assume that $\boldsymbol{\mathcal{R}}$ is the residual tensor, i.e., the difference between the left-hand side and the right-hand side of the (26) [or (27)]. The TS-SLS iteration stops either when the number of iterations reaches the maximum limit or when the higher-order norm of $\boldsymbol{\mathcal{R}}$ does not change between iterations by more than 10^{-10}. The signal-to-noise ratio (SNR) is defined as

$$\text{SNR}=\frac{E\{|s_k(n)|^2\}}{\sigma^2}.$$

We modeled the source signals as a zero mean circularly symmetric complex Gaussian random process. We therefore plot the unconditional or stochastic CRBs, CRB(μ) and CRB(η) in all the figures. The stochastic CRB can be achieved only for an infinite number of observations N[21], whereas we always consider a small number of observations. That is why the accuracy of TB-SS is far from CRB even though it is much better than the algorithms available in the literature.

A. Damped Harmonics

RMSEs in the normalized frequency and the damping factor are plotted for a damped harmonic retrieval problem with $M=15$, $M_{\rm sub}=8$, $L=8$, $N=8$, and SNR $=15$ dB in Fig. 3(a) and (b), respectively. The number of exponentials d is varied from 3 to 6. The separation between the exponentials in terms of the normalized frequency, i.e., $\Delta\mu$, is 0.5 and in terms of the damping factor, i.e., $\Delta\eta$, is 0.05. RMSE for SS with 1-D ESPRIT and TLS is the worst among the five scenarios. It is evident that the approach from [7] is better than the SS with 1-D ESPRIT and TLS approach for all values of d. This improvement is due to a better estimate of the subspace spanned by the matrix $\boldsymbol{A}_s$ obtained via the HOOI algorithm than that obtained via singular value decomposition (SVD) of the matrix $\boldsymbol{X}_{\rm ss}$. The tensor-based approaches, namely TB-SS with Tensor-ESPRIT and LS and TB-SS with Tensor-ESPRIT and TS-SLS provide a significantly better performance than the matrix-based approaches, namely 1-D ESPRIT and 2-D ESPRIT and the method from [7], at all values of d. The HOOI algorithm is used to estimate the tensor-based signal subspace estimate $\boldsymbol{\mathcal{U}}^{[s]}$. The two tensor-based approaches provide an almost same performance at $d=3$. As d increases, the improvement of TB-SS with Tensor-ESPRIT and TS-SLS over TB-SS with Tensor-ESPRIT and LS increases. This improvement is due to the fact that the TS-SLS algorithm provides a better estimate of the matrix $\boldsymbol{\Psi}$ than that provided by the LS algorithm.

Fig. 3(c) and (d) show the RMSEs in the normalized frequency and the damping factor versus the number of exponentials d when 1) the HOOI algorithm is used to estimate the tensor-based signal subspace estimate $\boldsymbol{\mathcal{U}}^{[s]}$ and 2) the truncated HOSVD is used to estimate the tensor $\boldsymbol{\mathcal{U}}^{[s]}$. The quality of estimate obtained via the HOOI algorithm is better, as evident from Fig. 3(c) and (d), though the improvement is very small. Also note that the improvement in RMSE by using TS-SLS instead of LS is significant, more so when the number of exponentials d is large.

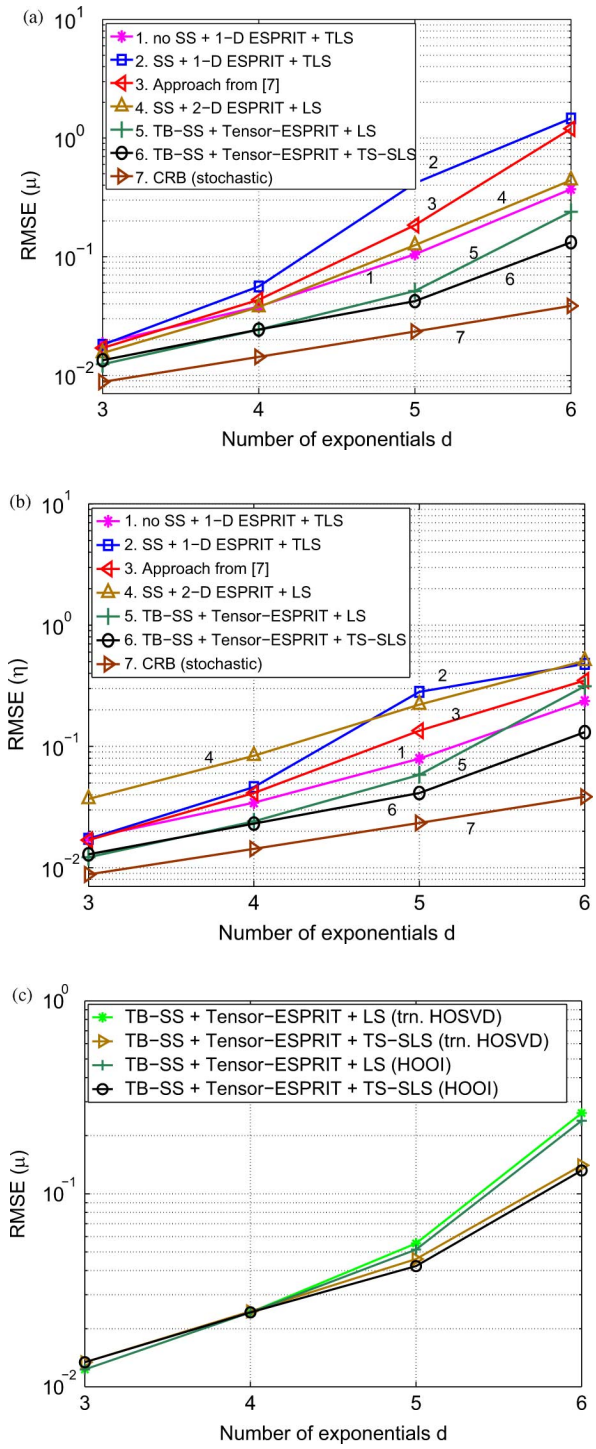

Fig. 3. (a) RMSE in μ for $M = 15$, $M_{\text{sub}} = 8$, $L = 8$, $N = 8$, SNR $= 15$ dB, $\Delta\mu = 0.5$, damped harmonics using HOOI. (b) RMSE in η for $M = 15$, $M_{\text{sub}} = 8$, $L = 8$, $N = 8$, SNR $= 15$ dB, $\Delta\eta = 0.05$, damped harmonics using HOOI. (c) Comparison between RMSE in μ for $M = 15$, $M_{\text{sub}} = 8$, $L = 8$, $N = 8$, SNR $= 15$ dB, $\Delta\mu = 0.5$, damped harmonics using HOOI and truncated HOSVD.

Fig. 3(e) is the plot of largest principal angle (LPA) versus the number of exponentials, d. The two curves correspond to the LPA between the matrix $\boldsymbol{C}_s$ and the signal subspace estimate obtained in 2-D standard ESPRIT $\boldsymbol{V}_3^{*[s]}$, and the LPA between the matrix $\boldsymbol{C}_s$ and the signal subspace estimate obtained in TB-SS $[\boldsymbol{\mathcal{U}}^{[s]}]_{(3)}^T$. The parameters used in the simulation are $M = 15$, $M_{\text{sub}} = 8$, $N = 8$, SNR $= 20$ dB, $\Delta\mu = 0.5$, $\Delta\eta = 0.05$. The number of exponentials d is varied from 2 to 6.

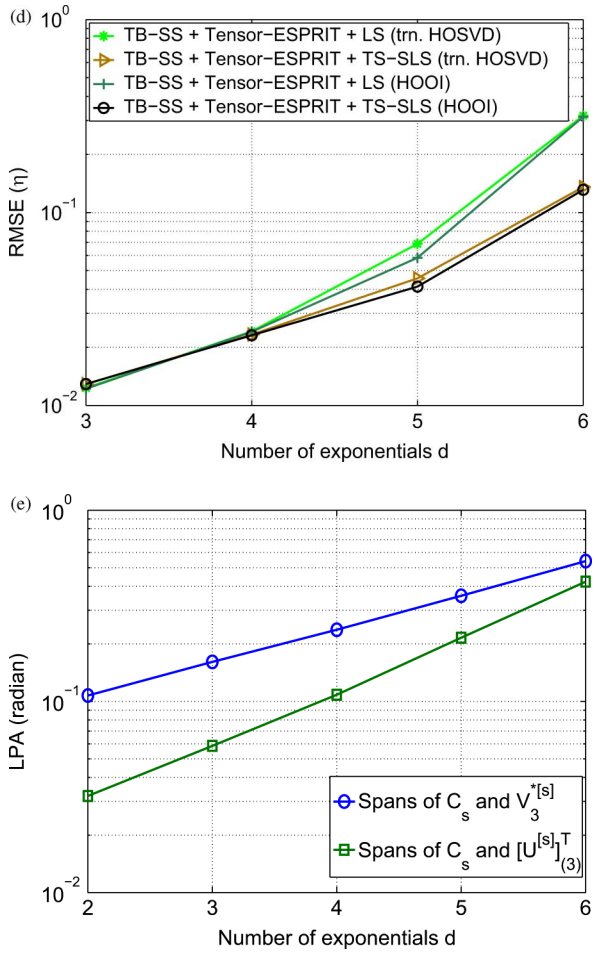

Fig. 3. (d) Comparison between RMSE in η for $M = 15$, $M_{\text{sub}} = 8$, $L = 8$, $N = 8$, SNR $= 15$ dB, $\Delta\eta = 0.05$, damped harmonics using HOOI and truncated HOSVD. (e) LPA for $M = 15$, $M_{\text{sub}} = 8$, $L = 8$, $N = 8$, SNR $= 15$ dB, $\Delta\mu = 0.5$, $\Delta\eta = 0.05$, damped harmonics.

Due to the lack of space, in the rest of this section, we present only those simulation results where the HOOI algorithm is used to estimate the tensor-based signal subspace estimate $\boldsymbol{\mathcal{U}}^{[s]}$. As already mentioned, the degradation in the RMSE by using the truncated HOSVD instead of the HOOI algorithm to estimate the tensor $\boldsymbol{\mathcal{U}}^{[s]}$ is very small. However, the computational complexity of the truncated HOSVD is significantly lower and therefore it is preferred over the HOOI algorithm in scenarios requiring a low computational complexity.

Fig. 4(a) and (b) depicts the RMSEs in the normalized frequency and the damping factor versus the number of channels N for $M = 15$, $M_{\text{sub}} = 8$, $L = 8$, and SNR $= 20$ dB. There are five complex exponentials with normalized frequencies and damping factors given in Table IV. As expected, TB-SS with standard Tensor-ESPRIT and TS-SLS results in the lowest RMSE at all values of N. The approach from [7] is better than SS with standard ESPRIT and TLS approach at all values of N. This is because the estimate of $\boldsymbol{U}_1^{[s]}$ obtained from $\boldsymbol{\mathcal{X}}$ via the HOOI algorithm in [7] is better than the estimate of $\boldsymbol{U}_1^{[s]}$ obtained by applying SVD on the matrix $\boldsymbol{X}_{\text{ss}}$. The tensor-based approaches perform significantly better than all other approaches

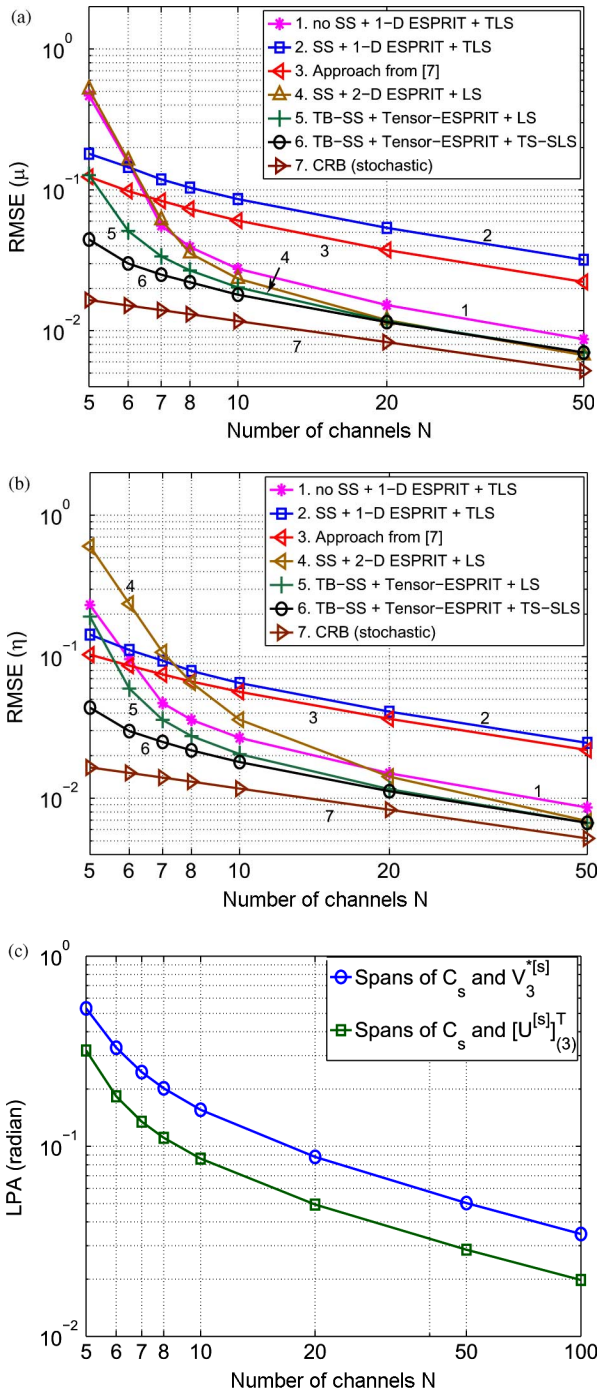

Fig. 4. (a) RMSE in μ for $M = 15$, $M_{\text{sub}} = 8$, $L = 8$, $d = 5$, SNR $= 20$ dB, $\Delta\mu = 0.5$, damped harmonics using HOOI. (b) RMSE in η for $M = 15$, $M_{\text{sub}} = 8$, $L = 8$, $d = 5$, SNR $= 20$ dB, $\Delta\eta = 0.05$, damped harmonics using HOOI. (c) LPA for $M = 15$, $M_{\text{sub}} = 8$, $L = 8$, $d = 5$, SNR $= 20$ dB, $\Delta\mu = 0.5$, $\Delta\eta = 0.05$, damped harmonics.

at all values of N, more so when the number of channels N is small. 2-D ESPRIT applied to the matrix $[\boldsymbol{\mathcal{X}}]_{(3)}^{T}$ gives a performance similar to tensor-based approaches at large values of N. The approach without SS and standard ESPRIT and TLS is worst among the six scenarios when the number of channels N is same as the number of exponentials d. It is interesting to note that this approach is better than SS with standard ESPRIT and TLS as well as the approach from [7] at $N \geq 7$, i.e., when the number of channels N is significantly higher than the number

TABLE IV
PARAMETERS OF DAMPED HARMONICS USED IN FIG. 4(A) AND (B)

Exponential	Normalized Frequency	Damping Factor
1	-0.8	-0.01
2	-0.3	-0.06
3	0.2	-0.11
4	0.7	-0.16
5	1.2	-0.21

of exponentials d. This behavior indicates that the standard spatial smoothing does not lead to an improvement in the estimation of the unknown parameters when the number of channels or independent observations is high. Spatial smoothing reduces the effective number of samples per channel and that is why the performance without spatial smoothing becomes better than the performance of SS with standard ESPRIT and TLS for large N. However, the tensor-based approaches, proposed in this paper, are better than not applying spatial smoothing at all values of N.

Fig. 4(c) is the plot of largest principal angle (LPA) versus the number of channels, N. The HOSVD algorithm is used to estimate the tensor $\boldsymbol{\mathcal{U}}^{[s]}$. The parameters used in the simulation are $M = 15$, $M_{\text{sub}} = 8$, $d = 8$, SNR $= 20$ dB, $\Delta\mu = 0.5$, $\Delta\eta = 0.05$. The number of channels d is varied from 5 to 100. The signal subspace estimate obtained in tensor-based methods is always a better estimate of the true signal subspace compared to that obtained in 2-D standard ESPRIT.

Fig. 5(a) and (b) shows the RMSEs in the normalized frequency and the damping factor when the number of subarrays, L, is varied keeping the number of samples per channel, M, the same. The SS with 1-D ESPRIT and TLS approach estimates the unknown parameters from a noisy matrix $\boldsymbol{X}_{\text{ss}}$ of size $M_{\text{sub}} \times NL$, the SS with 2-D ESPRIT and LS approach works with a matrix of size $M_{\text{sub}}L \times N$, while the tensor-based approaches estimate the unknown parameters from a noisy tensor $\boldsymbol{\mathcal{X}}$ of size $M_{\text{sub}} \times L \times N$. The simulation is performed for $d = 6$ exponentials, $N = 7$ channels, $M = 16$ samples per channel and 30 dB SNR. The unknown parameters are given in Table V. TB-SS with Tensor-ESPRIT and TS-SLS results in the smallest RMSE at all values of L. Moreover, this approach does not depend on the value of L (or M_{sub}) provided $M_{\text{sub}} \geq (d+1)$ (or $L \geq (d+1)$). The SS with standard ESPRIT and TLS approach and the approach from [7] depend heavily on the value of L.

Fig. 6(a) and (b) is the RMSE in the normalized frequency versus SNR and the RMSE in the damping factor versus the SNR plot when data from $N = 6$ different channels with each having $M = 17$ samples is used to estimate the parameters of $d = 5$ damped exponentials. The normalized frequencies and the damping factors of the 5 exponentials are given in Table IV. The number of subarrays, L, is 9. The matrix $\boldsymbol{X}_{\text{ss}}$ is of size 9×54, the matrix $[\boldsymbol{\mathcal{X}}]_{(3)}^{T}$ is of size 81×6, and the tensor $\boldsymbol{\mathcal{X}}$ is of size $9 \times 9 \times 6$. TB-SS with Tensor-ESPRIT and TS-SLS results in the least RMSE among the five scenarios at all values of SNR.

Fig. 7(a) and (b) shows the RMSEs in the normalized frequency and the damping factor versus the separation between normalized frequencies, i.e., $\Delta\mu$ of the d exponentials, respectively. The unknown parameters corresponding to $\Delta\mu = 0.3$ are given in Table VI. The other parameters used in simulation are

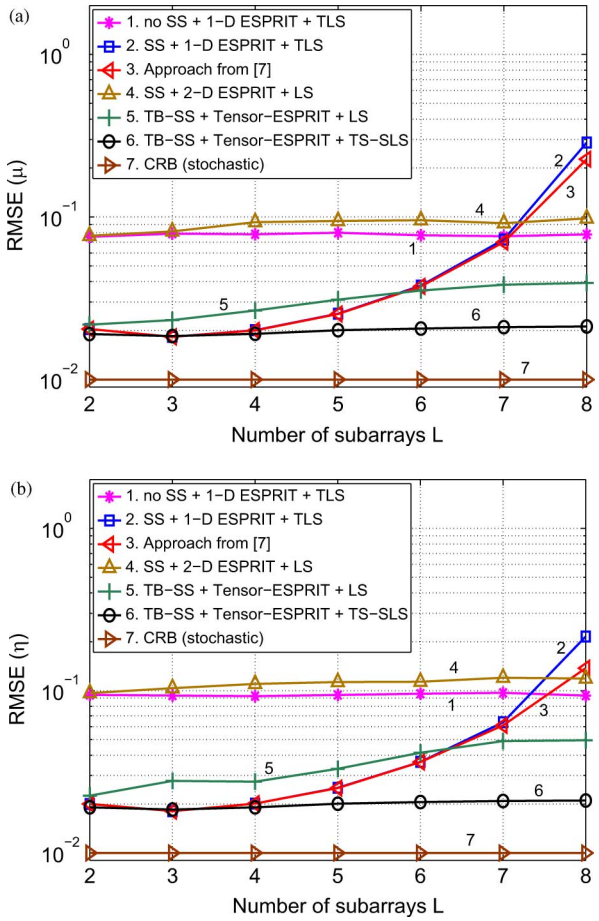

Fig. 5. (a) RMSE in μ for $M = 16$, $d = 6$, $N = 7$, SNR $= 30$ dB, $\Delta\mu = 0.4$, damped harmonics using HOOI. (b) RMSE in η for $M = 16$, $d = 6$, $N = 7$, SNR $= 30$ dB, $\Delta\eta = 0.05$, damped harmonics using HOOI.

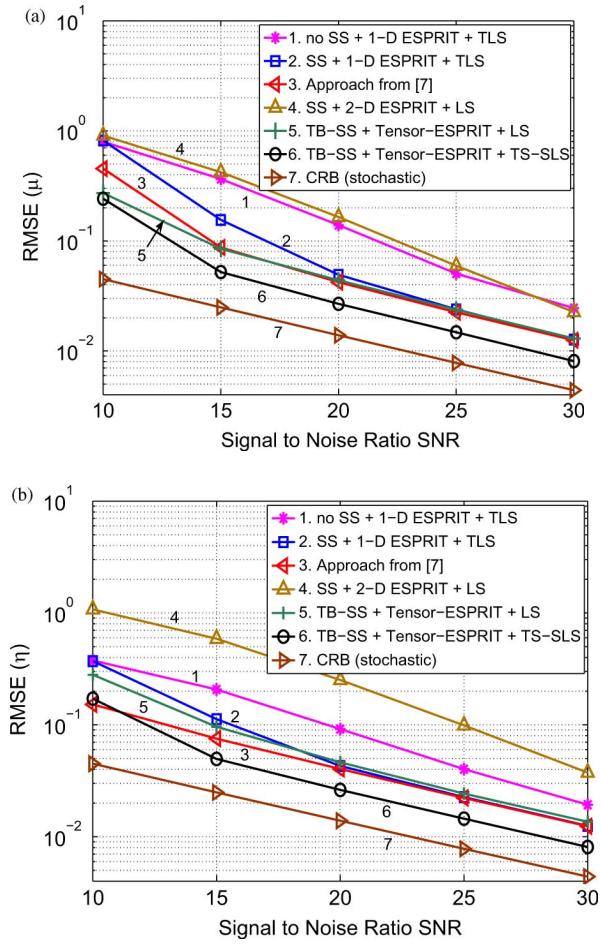

Fig. 6. (a) RMSE in μ for $M = 17$, $N = 6$, $d = 5$, $M_{\text{sub}} = 9$, $L = 9$, $\Delta\mu = 0.5$, damped harmonics using HOOI. (b) RMSE in η for $M = 17$, $N = 6$, $d = 5$, $M_{\text{sub}} = 9$, $L = 9$, $\Delta\eta = 0.05$, damped harmonics using HOOI.

TABLE V
PARAMETERS OF DAMPED EXPONENTIALS USED IN FIG. 5(A) AND (B)

Exponential	Normalized Frequency	Damping Factor
1	0.1	-0.01
2	0.5	-0.06
3	0.9	-0.11
4	1.3	-0.16
5	1.7	-0.21
6	2.1	-0.26

$M = 17$, $d = 5$, $N = 7$, $M_{\text{sub}} = 9$, and SNR $= 20$ dB. The simulation result shows that TB-SS with Tensor-ESPRIT and TS-SLS gives the best performance among the six scenarios at small values of $\Delta\mu$. Thus the ability of TB-SS with Tensor-ESPRIT and TS-SLS to resolve closely spaced exponentials is significantly better than the other four techniques. Note that the SS with 1-D ESPRIT and TLS approach and the approach from [7] are the best among the five scenarios when $\Delta\mu = 0.7, 0.8$, i.e., when the d exponentials have normalized frequencies that are wide apart.

Fig. 8(a) and (b) shows the RMSEs in the normalized frequency and the damping factor versus the separation between damping factors, i.e., $\Delta\eta$ of the d exponentials, respectively. Simulations are performed for $d = 5$ exponentials, $N = 7$ channels, $M = 15$ samples per channel and at 20 dB SNR. The number of subarrays L is chosen to be 8. The normalized frequencies and the damping factors of the five exponentials when $\Delta\eta = -0.01$ and $\Delta\eta = -0.13$ are given in Tables VII and VIII, respectively. The normalized frequencies of the five exponentials are kept the same at all values of $\Delta\eta$. The RMSE increases with an increase in the absolute values of the damping factors, i.e., with the decrease in magnitudes of the exponentials. It is evident from the plots that TB-SS with Tensor-ESPRIT and TS-SLS gives the best performance among all the six scenarios at all values of $\Delta\eta$. The improved performance shown by TB-SS with Tensor-ESPRIT and TS-SLS approach is due to the following three factors: 1) a better estimate of the signal subspace provided by $\boldsymbol{U}^{[s]}$ over $\boldsymbol{V}_3^{*[s]}$; 2) a further improvement in $\boldsymbol{U}^{[s]}$ provided by the TS-SLS algorithm leading to a better estimate of $\boldsymbol{\Psi}$ over the LS algorithm; and 3) a larger number of equations to be solved for the same number of unknowns d.

B. Undamped Harmonics

Due to the lack of space, we present a selected few simulation results for an undamped harmonic retrieval problem in this section. Unitary ESPRIT is used to estimate the unknown normalized frequencies (or spatial frequencies in case of DOA estimation problem) from the spatially smoothed matrix $\boldsymbol{X}_{\text{ss}}$ with the restrictions $M_{\text{sub}} \geq (d+1)$ and $NL/2 \geq d$. Unitary

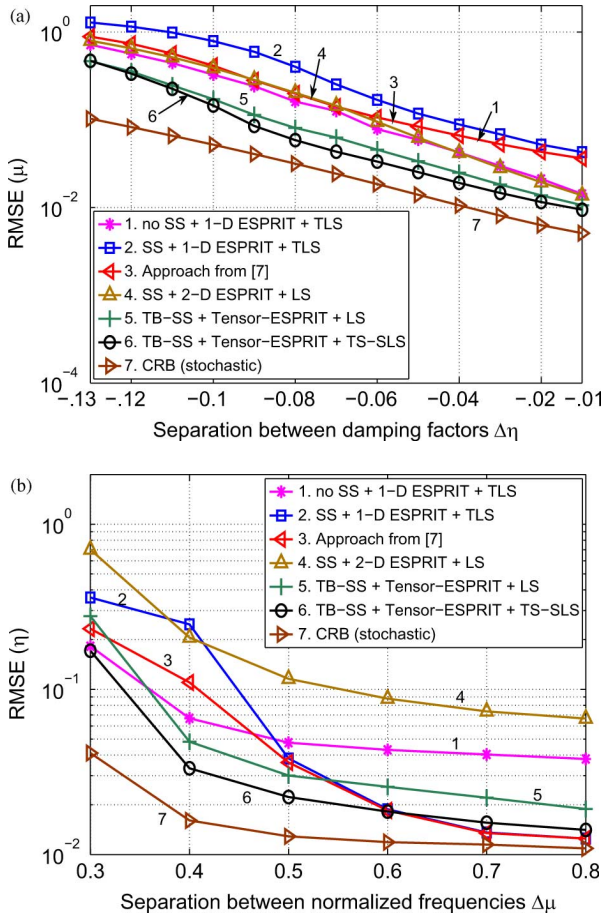

Fig. 7. (a) RMSE in μ for $M = 17$, $N = 7$, $d = 5$, $M_{\text{sub}} = 9$, $L = 9$, SNR $= 20$ dB, $\Delta\eta = 0.05$, damped harmonics using HOOI. (b) RMSE in η for $M = 17$, $N = 7$, $d = 5$, $M_{\text{sub}} = 9$, $L = 9$, SNR $= 20$ dB, $\Delta\eta = 0.05$, damped harmonics using HOOI.

TABLE VI
PARAMETERS USED IN FIG. 7(A) AND (B) FOR $\Delta\mu = 0.3$

Exponential	Normalized Frequency	Damping Factor
1	0.1	-0.01
2	0.4	-0.06
3	0.7	-0.11
4	1.0	-0.16
5	1.3	-0.21

Tensor-ESPRIT is used to estimate the normalized frequencies from the measurement tensor $\boldsymbol{\mathcal{X}}$ with the restriction $N/2 \geq d$ and assuming one of the following two conditions to be true: (i) $M_{\text{sub}} \geq (d+1)$, (ii) $L \geq (d+1)$. Results obtained by applying Unitary ESPRIT to the measurement matrix $\boldsymbol{X}$ are also presented here.

Fig. 9 shows the RMSE in the normalized frequency vs. the number of exponentials plot at an SNR of 20 dB using data from $N = 3$ channels with each channel having $M = 13$ samples. The length of the subarray, M_{sub}, is chosen to be 7. The effective number of channels gets doubled to 6 as a result of applying Unitary ESPRIT or Unitary Tensor-ESPRIT. The SS with Unitary ESPRIT and LS, the SS with Unitary ESPRIT and TLS as well as TB-SS with Unitary ESPRIT and TLS estimate the normalized frequencies from a real-valued matrix-based subspace estimate of dimensions $7 \times d$ while TB-SS with Unitary

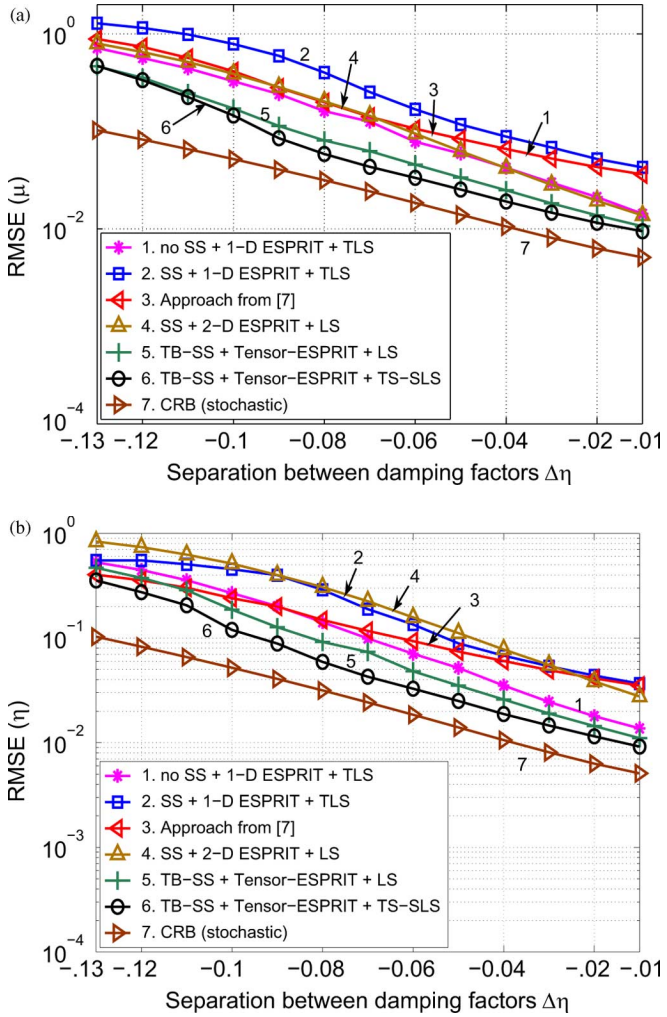

Fig. 8. (a) RMSE in μ for $M = 15$, $N = 7$, $d = 5$, $M_{\text{sub}} = 8$, $L = 8$, SNR $= 20$ dB, $\Delta\mu = 0.5$, damped harmonics using HOOI. (b) RMSE in η for $M = 15$, $N = 7$, $d = 5$, $M_{\text{sub}} = 8$, $L = 8$, SNR $= 20$ dB, $\Delta\mu = 0.5$, damped harmonics using HOOI.

TABLE VII
PARAMETERS USED IN FIG. 8(A) AND (B) FOR $\Delta\eta = -0.01$

Normalized Frequency, μ	Damping Factor, η	Magnitude, e^{η}
-1.05	-0.01	0.9900
-0.55	-0.02	0.9802
-0.05	-0.03	0.9704
0.45	-0.04	0.9608
0.95	-0.05	0.9512

Tensor-ESPRIT and LS approach as well as TB-SS with Unitary Tensor-ESPRIT and TS-SLS approach estimate the normalized frequencies from a real-valued tensor-based subspace estimate of dimensions $7 \times 7 \times d$ using the HOOI algorithm. The normalized frequencies to be estimated are given in Table IX. SS with Unitary ESPRIT and LS provides a performance similar to that obtained by SS with Unitary ESPRIT and TLS in spite of the fact that TLS is computationally more expensive than LS. The tensor-based approaches exhibit a superior performance than the

TABLE VIII
PARAMETERS USED IN FIG. 8(A) AND (B) FOR $\Delta\eta = -0.13$

Normalized Frequency, μ	Damping Factor, η	Magnitude, e^{η}
-1.05	-0.01	0.9900
-0.55	-0.14	0.8694
-0.05	-0.27	0.7634
0.45	-0.40	0.6703
0.95	-0.53	0.5886

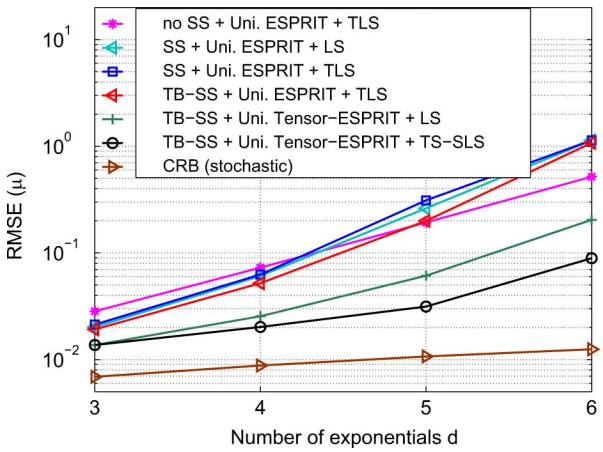

Fig. 9. RMSE for $M = 13$, $N = 3$, $M_{\text{sub}} = 7$, $L = 7$, SNR $= 20$ dB, $\Delta\mu = 0.5$, undamped harmonics using HOOI.

TABLE IX
PARAMETERS OF UNDAMPED EXPONENTIALS USED IN FIG. 9

No. of Exponentials, d	Normalized Frequencies
3	-0.5, 0, 0.5
4	-1, -0.5, 0, 0.5
5	-1, -0.5, 0, 0.5, 1
6	-1.5, -1, -0.5, 0, 0.5, 1

matrix-based approaches at all values of d. The reason for the superior performance is the better estimate of the signal subspace provided by the tensor $\mathcal{E}^{[s]}$ in the presence of noise.

Fig. 10(a) is the RMSE in the normalized frequency vs. the number of subarrays L plot when $d = 7$ normalized frequencies, $\mu_1 = -0.8$, $\mu_2 = -0.4$, $\mu_3 = 0$, $\mu_4 = 0.4$, $\mu_5 = 0.8$, $\mu_6 = 1.2$, and $\mu_7 = 1.6$, are estimated using data from the output of $N = 4$ channels with each channel having $M = 15$ samples at 15 dB SNR. TB-SS with Unitary Tensor-ESPRIT and LS and TB-SS with Unitary Tensor-ESPRIT and TS-SLS exhibit a similar and the best performance in terms of RMSE at all values of L. This is due to the fact that the real-valued tensor $\mathcal{E}^{[s]}$ is a better estimate of the subspace spanned by the tensor $\mathcal{A} \times_1 \boldsymbol{Q}^H_{M_{\text{sub}}} \times_2 \boldsymbol{Q}^H_L$ than the estimate of the subspace spanned by $\boldsymbol{Q}^H_{M_{\text{sub}}} \cdot \boldsymbol{A}_s$ provided by the real-valued matrix $\boldsymbol{E}^{[s]}_1$. TB-SS with Unitary ESPRIT and TLS performs slightly better than or equal to SS with Unitary ESPRIT and TLS approach at all values of L because of improvement provided by the HOOI algorithm. Note that the TS-SLS algorithm is better than the LS

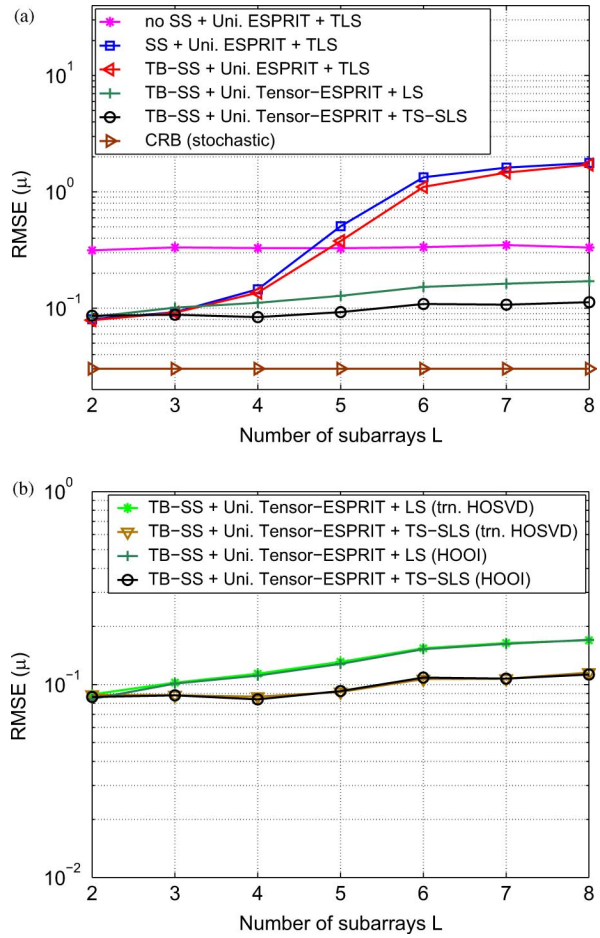

Fig. 10. (a) RMSE for $M = 15$, $d = 7$, SNR $= 15$ dB, $N = 4$, $\Delta\mu = 0.4$, undamped harmonics using HOOI. (b) Comparison between RMSE for $M = 15$, $d = 7$, SNR $= 15$ dB, $N = 4$, $\Delta\mu = 0.4$, undamped harmonics using HOOI and truncated HOSVD.

algorithm leading to a significant improvement in the RMSE. In addition, the tensor-based approaches give RMSEs that stay almost the same at different values of L. RMSEs obtained in the matrix-based approaches, i.e., SS with Unitary ESPRIT and TLS approach and TB-SS with Unitary ESPRIT and TLS approach increase by a factor of more than 10 as L increases from 2 to 8 (or M_{sub} decreases from 14 to 8).

Fig. 10(b) depicts the RMSE in the normalized frequency versus the number of subarrays where 1) the truncated HOSVD and 2) the HOOI algorithm are used to estimate the signal subspace from the tensor $\varphi(\mathcal{X})$. Here, the RMSE obtained by using the HOOI algorithm is same as the RMSE obtained by using the truncated HOSVD algorithm.

X. CONCLUSION

TB-SS is a preprocessing technique for subspace-based parameter estimation of one-dimensional damped and undamped harmonics. TB-SS packs noisy data from the output of multiple channels into a measurement tensor. Next a tensor-based subspace estimate is constructed from the measurement tensor in a way such that the multidimensional invariance property exhibited by the measurement tensor is fully exploited. This tensor-based subspace estimate in conjunction with ESPRIT-type algorithms performs significantly better than

$$\boldsymbol{\beta}^T = \Big[\mu_1, \mu_2, \ldots, \mu_d, \eta_1, \ldots, \eta_d, [\boldsymbol{R}_s]_{1,1}, [\boldsymbol{R}_s]_{2,2}, \ldots, \mathrm{Re}([\boldsymbol{R}_s]_{1,2}), \mathrm{Im}([\boldsymbol{R}_s]_{1,2}), \ldots, \mathrm{Re}([\boldsymbol{R}_s]_{d-1,d}), \mathrm{Im}([\boldsymbol{R}_s]_{d-1,d}), \sigma^2\Big] \quad \in \mathbb{R}^{(2d+d^2+1)\times 1} \tag{44}$$

existing subspace estimates reported in literature in conjunction with ESPRIT-type algorithms in all investigated scenarios. The advantage of the tensor-based approaches over the existing approaches is more significant when (a) the number of channels N is nearly equal to the number of exponentials d, and (b) the exponentials are closely spaced in terms of their normalized frequencies. In addition, the proposed tensor-based approach is insensitive to changes in the number of samples per subarray, M_{sub}, provided that the number of subarrays, L is greater than the number of exponentials d. TB-SS is also insensitive to changes in L provided that $M_{\mathrm{sub}} \geq (d+1)$. TB-SS is applicable when the number of channels is at least equal to the number of harmonics in damped harmonic retrieval problems and at least equal to half the number of harmonics in case of undamped harmonic retrieval problems. Among the two tensor-based approaches, namely TB-SS with Tensor-ESPRIT (Unitary Tensor-ESPRIT) and LS, and TB-SS with Tensor-ESPRIT (Unitary Tensor-ESPRIT) and TS-SLS, the second one provides a better performance in terms of the RMSE, particularly in critical scenarios. This improvement is due to the superior performance of the TS-SLS algorithm over the LS algorithm. However the computational complexity of TS-SLS is significantly higher than the LS algorithm. Therefore, the computational complexity can be reduced by using TB-SS with Tensor-ESPRIT and LS. The computational complexity can be further reduced by replacing the HOOI algorithm with the truncated HOSVD to find a low-rank approximation of the measurement tensor $\boldsymbol{\mathcal{X}}$. The degradation in the RMSE performance due to the use of the truncated HOSVD is insignificantly small. The 1-D TB-SS presented here can be extended to the R-dimensional (R-D) estimation of damped and undamped harmonics and R-D direction-of-arrival estimation.

APPENDIX

Let $\boldsymbol{a}_k$ and $\boldsymbol{c}_k$ denote the kth column of the matrix $\boldsymbol{A}$ and the matrix $\boldsymbol{R}_s$, respectively.

$$\boldsymbol{A} = [\boldsymbol{a}_1, \ldots, \boldsymbol{a}_d], \quad \boldsymbol{R}_s = [\boldsymbol{c}_1, \ldots, \boldsymbol{c}_d].$$

Following are the definitions of some parameters used here: see (44) at the top of the page.

$$\boldsymbol{R}_x = \boldsymbol{A}\boldsymbol{R}_s\boldsymbol{A}^H + \sigma^2\boldsymbol{I}_M,$$
$$\boldsymbol{P}_{\boldsymbol{A}} = (\boldsymbol{I}_M - \boldsymbol{A}(\boldsymbol{A}^H\boldsymbol{A})^{-1}\boldsymbol{A}^H), \quad \boldsymbol{R}_s = \boldsymbol{I}_d.$$

For $k = 1, 2, \ldots, d$,

$$\frac{\partial \boldsymbol{R}_x}{\partial [\boldsymbol{\beta}]_k} = \left(\frac{\partial \boldsymbol{a}_k}{\partial [\boldsymbol{\beta}]_k}\right)\boldsymbol{c}_k^H\boldsymbol{A}^H + \boldsymbol{A}\boldsymbol{c}_k\left(\frac{\partial \boldsymbol{a}_k}{\partial [\boldsymbol{\beta}]_k}\right)^H. \tag{45}$$

For $k = d+1, d+2, \ldots, 2d$

$$\frac{\partial \boldsymbol{R}_x}{\partial [\boldsymbol{\beta}]_k} = \left(\frac{\partial \boldsymbol{a}_{(k-d)}}{\partial [\boldsymbol{\beta}]_k}\right)\boldsymbol{c}_{(k-d)}^H\boldsymbol{A}^H + \boldsymbol{A}\boldsymbol{c}_{(k-d)}\left(\frac{\partial \boldsymbol{a}_{(k-d)}}{\partial [\boldsymbol{\beta}]_k}\right)^H. \tag{46}$$

We define $r = \mod(k-1, d) + 1$. Then, for $k = 1, 2, \ldots, 2d$

$$\frac{\partial \boldsymbol{R}_x}{\partial [\boldsymbol{\beta}]_k} = \left(\frac{\partial \boldsymbol{a}_r}{\partial [\boldsymbol{\beta}]_k}\right)\boldsymbol{c}_r^H\boldsymbol{A}^H + \boldsymbol{A}\boldsymbol{c}_r\left(\frac{\partial \boldsymbol{a}_r}{\partial [\boldsymbol{\beta}]_k}\right)^H. \tag{47}$$

Following the derivation given in [20], we get for $p = 1, 2, \ldots, 2d$, and for $k = 1, 2, \ldots, 2d$

$$[\,\mathrm{CRB}^{-1}(\boldsymbol{\beta})]_{p,k} = \frac{2N}{\sigma^2} \cdot \mathrm{Re}\left(\left(\left(\frac{\partial \boldsymbol{a}_t}{\partial [\boldsymbol{\beta}]_p}\right)^H \boldsymbol{P}_{\boldsymbol{A}}\left(\frac{\partial \boldsymbol{a}_r}{\partial [\boldsymbol{\beta}]_k}\right)\right) \cdot \left(\boldsymbol{c}_r^H\boldsymbol{A}^H\boldsymbol{R}_x^{-1}\boldsymbol{A}\boldsymbol{c}_t\right)\right) \tag{48}$$

where $t = \mod(p-1, d) + 1$. With the matrices $\boldsymbol{R}_{\mathrm{ss}}$ and $\boldsymbol{D}$ defined in Section VIII

$$[\,\mathrm{CRB}^{-1}(\boldsymbol{\beta})]_{p,k} = \frac{2N}{\sigma^2} \cdot \mathrm{Re}\left\{[\boldsymbol{D}^H\boldsymbol{P}_{\boldsymbol{A}}\boldsymbol{D}]_{p,k} \cdot \left[\boldsymbol{R}_{\mathrm{ss}}^T\boldsymbol{A}^H\boldsymbol{R}_x^{-1}\boldsymbol{A}\boldsymbol{R}_{\mathrm{ss}}\right]_{k,p}\right\}. \tag{49}$$

Equation (43) follows immediately from (49).

ACKNOWLEDGMENT

The authors gratefully acknowledge the fruitful discussions with L. Lathauwer that helped to improve the manuscript considerably. Also, the authors would like to express their gratitude to L. Lathauwer for providing a MATLAB implementation of the HOOI algorithm.

REFERENCES

[1] M. Pesavento, S. Shahbazpanahi, J. F. Boehme, and A. B. Gershman, "Exploiting multiple shift invariances in multidimensional harmonic retrieval of damped exponentials," in *Proc. IEEE Int. Conf. Acoust., Speech, Signal Process.*, 2005, pp. 1017–1020.

[2] J. E. Evans, D. F. Sun, and J. R. Johnson, "Application of advanced signal processing techniques to angle of arrival estimation in ATC navigation and surveillance systems," M.I.T. Lexington Lincoln Lab., Lexington, MA, 1982.

[3] T.-J. Shan, M. Wax, and T. Kailath, "On spatial smoothing for direction-of-Arrival estimation of coherent signals," *IEEE Trans. Acoust., Speech, Signal Process.*, vol. 33, no. 4, pp. 806–811, Aug. 1985.

[4] R. Roy and T. Kailath, "ESPRIT—Estimation of signal parameters via rotational invariance techniques," *IEEE Trans. Acoust., Speech, Signal Process.*, vol. 37, no. 7, pp. 984–995, Jul. 1989.

[5] M. Haardt, "Efficient one-, two-, and multidimensional high-resolution array signal processing," Ph.D. dissertation, Technical Univ. Munich, Aachen, 1997.

[6] M. Haardt and J. Nossek, "Unitary ESPRIT: How to obtain increased estimation accuracy with a reduced computational burden," *IEEE Trans. Signal Process.*, vol. 43, no. 5, pp. 1232–1242, May 1995.
[7] J. M. Papy, L. de Lathauwer, and S. van Huffel, "Exponential data fitting using multilinear algebra: The single-channel and the multi-channel case," *Numer. Linear Algebra Appl.*, vol. 21, pp. 809–826, 2005.
[8] A.-J. V. D. Veen, E. F. Deprettere, and A. L. Swindlehurst, "Subspace-based signal analysis using singular value decomposition," *IEEE Signal Process. Lett.*, pp. 1277–1308, Sep. 1993.
[9] M. Haardt, F. Roemer, and G. Del Galdo, "Higher-order SVD-based subspace estimation to improve the parameter estimation accuracy in multidimensional harmonic retrieval problems," *IEEE Trans. Signal Process.*, vol. 56, no. 7, pp. 3198–3213, Jul. 2008.
[10] X. Liu and N. D. Sidiropoulos, "Almost sure identifiability of constant modulus multidimensional harmonic retrieval," *IEEE Trans. Signal Process.*, vol. 50, no. 9, pp. 2366–2368, Sep. 2002.
[11] T. Jiang, N. D. Sidiropoulos, and J. M. F. ten Berge, "Almost sure identifiability of multidimensional harmonic retrieval," in *Proc. IEEE Int. Conf. Acoust., Speech, Signal Process.*, 2001, pp. 3093–3096.
[12] R. Boyer, L. de Lathauwer, and K. Abed-Meraim, "Higher order tensor-based method for delayed exponential fitting," *IEEE Signal Process. Lett.*, pp. 2795–2809, Jun. 2007.
[13] S. Van Huffel, H. Chen, C. Decanniere, and P. Van Hecke, "Algorithm for time-domain NMR data fitting based on total least squares," *J. Magn. Reson. A*, vol. 110, pp. 228–237, Oct. 1994.
[14] A. Thakre, M. Haardt, and K. Giridhar, "Single snapshot spatial smoothing with improved effective array aperture," *IEEE Signal Process. Lett.*, pp. 505–508, Jun. 2009.
[15] L. de Lathauwer, B. de Moor, and J. Vanderwalle, "A multilinear singular-value decomposition," *SIAM J. Matrix Anal. Appl.*, vol. 21, no. 4, pp. 1253–1278, 2000.
[16] L. de Lathauwer, B. de Moor, and J. Vanderwalle, "On the best rank-1 and rank-$(r_1, r_2, \ldots, r_n)$ approximation of higher-order tensors," *SIAM J. Matrix Anal. Appl.*, vol. 21, no. 4, pp. 1324–1342, 2000.
[17] M. Haardt, "Structured least squares to improve the performance of ESPRIT-type algorithms," *IEEE Trans. Signal Process.*, vol. 45, no. 3, pp. 792–799, Mar. 1997.
[18] F. Roemer and M. Haardt, "Tensor-structure structured least squares to improve the performance of multi-dimensional ESPRIT-type algorithms," in *Proc. IEEE Int. Conf. Acoust., Speech, Signal Process.*, 2007, pp. 1324–1342.
[19] F. Roemer, H. Becker, M. Haardt, and M. Weis, "Analytical performance evaluation for HOSVD-based parameter estimation schemes," in *Proc. IEEE Int. Workshop on Comp. Adv. in Multi-Sensor Adaptive Process. (CAMSAP)*, 2009.
[20] P. Stoica, E. G. Larsson, and A. B. Gershman, "The stochastic CRB for array processing: A textbook derivation," *IEEE Signal Process. Lett.*, vol. 8, no. 5, pp. 148–150, May 2001.
[21] P. Stoica and A. Nehorai, "Performance study of conditional and unconditional direction-of-Arrival estimation," *IEEE Trans. Acoust., Speech, Signal Process.*, vol. 38, no. 10, pp. 1783–1795, Oct. 1990.

Arpita Thakre (S'04) received the Bachelor of Technology and Master of Technology degrees from the Institute of Radiophysics and Electronics, Kolkata, India, both with a major in communications engineering.

Since August 2005, she has been working as a Research Assistant with the Electrical Engineering Department, Indian Institute of Technology, Madras. Her current research interests include transceiver algorithms for next generation wireless systems, multidimensional signal processing, and multilinear algebra. She has also worked in the areas of cognitive radio while working at Honeywell Technology Solutions Lab, Bangalore, India, and MIMO communications while working at HelloSoft, Hyderabad, India. She has research contribution to IEEE 802.16 TGm. She was a visiting researcher with the Ilmenau University of Technology, Germany, during 2008–2009.

Martin Haardt (S'90–M'98–SM'99) received the Diplom-Ingenieur (M.S.) degree from the Ruhr-University Bochum, Germany, in 1991, and the Doktor-Ingenieur (Ph.D.) degree from Munich University of Technology, Munich, Germany, in 1996.

He has been a Full Professor with the Department of Electrical Engineering and Information Technology and Head of the Communications Research Laboratory, Ilmenau University of Technology, Germany, since 2001. In 1997, he joined Siemens Mobile Networks, Munich, where he was responsible for strategic research for third-generation mobile radio systems. From 1998 to 2001, he was the Director for International Projects and University Cooperations in the mobile infrastructure business of Siemens, where his work focused on mobile communications beyond the third generation. During his time at Siemens, he also taught in the international Master of Science in Communications Engineering program at Munich University of Technology. His research interests include wireless communications, array signal processing, high-resolution parameter estimation, as well as numerical linear and multilinear algebra.

Dr. Haardt has received the 2009 Best Paper Award from the IEEE Signal Processing Society, the Vodafone (formerly Mannesmann Mobilfunk) Innovations-Award for outstanding research in mobile communications, the ITG best paper award from the Association of Electrical Engineering, Electronics, and Information Technology (VDE), and the Rohde and Schwarz Outstanding Dissertation Award. In fall 2006 and fall 2007, he was a Visiting Professor with the University of Nice, Sophia-Antipolis, France, and with the University of York, U.K., respectively. He has served as an Associate Editor for the IEEE TRANSACTIONS ON SIGNAL PROCESSING (2002–2006), the IEEE SIGNAL PROCESSING LETTERS (since 2006), the *Research Letters in Signal Processing* (2007–2009), and the *Hindawi Journal of Electrical and Computer Engineering* (since 2009). He has also served as the Technical Co-Chair of the IEEE International Symposiums on Personal Indoor and Mobile Radio Communications (PIMRC) 2005 in Berlin, Germany, and as the Technical Program Chair of the IEEE International Symposium on Wireless Communication Systems 2010, York, U.K.

Florian Roemer (S'04) has studied computer engineering at Ilmenau University of Technology, Germany, and McMaster University, Canada. He received the Diplom-Ingenieur (M.S.) degree with a major in communications engineering in October 2006. For his diploma thesis, he received the Siemens Communications Academic Award 2006.

Since December 2006, he has been a Research Assistant with the Communications Research Laboratory, Ilmenau University of Technology. His research interests include multidimensional signal processing, high-resolution parameter estimation, as well as multiuser MIMO and relaying systems.

K. Giridhar received the B.Sc. degree in applied sciences from PSG College of Technology, Coimbatore, India, in 1985, the M.E. degree in electrical communication engineering from the Indian Institute of Science, Bangalore, in 1989, and the Ph.D. degree in electrical and communication engineering from the University of California, Santa Barbara, in 1993.

After working for a year as a Research Affiliate with Stanford University, Stanford, CA, he joined the Indian Institute of Technology, Madras, in 1994, where he is currently a Professor of electrical engineering. Being an active member of the TeNeT group (www.tenet.res.in), his research interests are in the areas of adaptive estimation with a focus on MIMO-OFDM wireless transceivers, and performance analysis of wireless networks. His research group also works closely with the Center of Excellence in Wireless Technology (www.cewit.org). He is a visiting faculty member with Sri Sathya Sai University, Prasanthi Nilayam, India.